Thermal Protection System P50 Cork Char Response Characterization to Ascent Flight Shear and Heating Environments

Manish Mehta[1*], David A. Brewer[1†], Jacob A. Parton[1‡] and Ron D. Beshears[1§]

[1]*NASA Marshall Space Flight Center, Huntsville, AL 35812*

NASA's Space Launch System (SLS) experienced deflagration of the acreage of the Core Stage base heat shield during the Green Run hot-fire test campaigns and Artemis I flight. The burning products from the base heat shield during Green Run hot-fire test operation led to concerns in aerothermal environments and thermal protection system (TPS) performance prior to Artemis I flight. Updated design thermal environments accounting for cork combustion were developed using Green Run measurements and assessed prior to Artemis I, resulting in increased TPS thickness for the base heat shield. This work documents a highly controlled ground test within the NASA Marshall Space Flight Center's Propulsion Test Branch Hot Gas Facility (HGF) and investigates the P50 cork TPS response due to sensitivity changes in radiative heat rates and surface shear stress. Prior to testing at the HGF, most of the P50 cork panels had a thick layer of char due to the cork combustion process replicated in a thermal vacuum chamber. SLS ascent shear stress and heating rate profile were simulated within the HGF by running the combustion-driven wind tunnel at off-nominal conditions and Mach numbers below 1. This test data provided insight into aerothermal measurements from Artemis I flight as well as informing updated base heating design environments for Artemis II. An in-depth understanding of the TPS P50 cork char response and observations is presented for launch vehicle flight ascent environments.

Nomenclature

Al	=	Aluminum	*Pr*	=	Prandtl Number
ATA-002	=	2% SLS base heating shock tunnel test	*qdotr*	=	radiative heat flux
BHS	=	base heat shield	*R*	=	gas constant
BFS	=	BTU/ft^2-sec	*Re*	=	Reynolds Number
BET	=	best estimated trajectory	ρ	=	density
CFD	=	computational fluid dynamics	*SLS*	=	Space Launch System
CS	=	SLS core-stage	τ	=	shear stress
C_f	=	skin friction coefficient	*T*	=	temperature
DFI	=	Development Flight Instrumentation	*TC*	=	thermocouple
γ	=	specific heat ratio	*TVC*	=	thermal vacuum chamber
GTP	=	gas temperature probe	*U*	=	velocity
HD	=	high definition	Subscript		
HGF	=	Hot-Gas Facility	0	=	total conditions
HF	=	Green Run Hot-Fire Test	*p*	=	plume
h	=	heat transfer coefficient	∞	=	freestream conditions
k	=	thermal conductivity	*s*	=	surface conditions
Ma	=	Mach Number	*PXX*	=	pressure DFI name
μ	=	gas viscosity	*T*	=	total heat rate
Nu	=	Nusselt Number	*R*	=	radiative heat rate
P	=	pressure	*rec*	=	recovery
P50	=	Phenolic resin cork with 50 *u*m granules	*W*	=	wall
psf	=	pounds-per-square-feet			

* Subject Matter Expert (SME), Aerosciences Branch, AIAA Senior Member, manish.mehta@nasa.gov

† Aerospace Engineer, Aerosciences Branch

‡ Branch Chief, Propulsion Test Branch

§ Subject Matter Expert (SME), Damage Tolerance Assessment Branch

I. Introduction

Artemis I was the first human-rated lunar system test flight since Apollo 5 in 1968 where the Saturn V launch vehicle carried the Service, Lunar, and Command Modules around the moon[1-3]. Artemis I was the first integrated test flight encompassing the Space Launch System (SLS) launch vehicle and the Orion spacecraft. Artemis I successfully launched from Pad39B from the Kennedy Space Center, Florida on November 16, 2022, as shown in Figure 1. The SLS was propelled with four liquid hydrogen (LH_2) and liquid oxygen (LO_2) rocket engines and two five-segment solid rocket boosters (SRB)[1-3].

There were various base TPS components for the SLS vehicle that were instrumental in protecting the base of the vehicle from excess heating during flight. The base heat shield (BHS) which is the largest aft-end acreage structure, protects the base of the vehicle and its internal components and avionics cabling from excessive plume-induced heating. Boeing was using P50 cork for the BHS which was coated with Hypalon paint. The engine-mounted heat shield (EMHS) protects RS-25 turbopump machinery and gimbal actuators. A thermal blanket was used for the EMHS. Thermal protection systems on the aft end are needed to encompass the total expanse of plume induced environments experienced over the duration of the ascent burn.

Figure 1 shows the Artemis I flight core-stage and SRB base region with all first-stage engines and solid rocket motors firing nominally[2-3]. The complex flow field can be seen with six rocket exhaust plumes and atmospheric air interacting in the SLS Core Stage and SRB base regions at T + 15 seconds. The T + 0 second point for Artemis I flight data analysis was defined at SRB ignition which occurred on November 16th, 2022, at 1:47:44 AM EST. All flight time in this report was with respect to this reference time. The SRB aluminum-oxide laden plumes were bright (near saturated pixels) while the RS-25 water vapor dominated plumes were relatively transparent. Along with the complex plume flow field, there was two-phase TPS – gas phenomena occurring on the surface of the heat shield during ascent which will be described in detail within this paper. This infrared (IR) imagery data (Figure 1) was captured by the MARS Scientific ground-based imager system which was part of the NASA Langley Research Center's Scientifically Calibrated In-Flight Imagery (SCIFLI) Team[5].

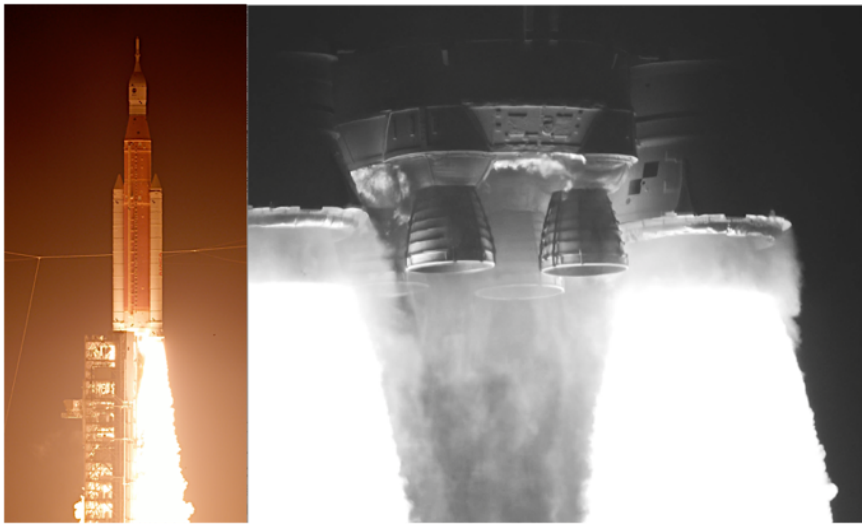

Figure 1. Artemis I SLS launch (left) and IR image of the SLS base at T+15 seconds (right)[2-3].

Figure 2 shows a large-scale combustion phenomena on the base heat shield which was first observed during SLS Core Stage Green Run Hot-Fire Test 1 and Hot-Fire Test 2 test series at flight-scales[1]. The cork combustion dynamics were first seen in 2017 through visible imagery in some precursor sea-level sub-scale ground tests at the NASA Marshall Space Flight Center's Nonmetallic Materials and Space Environmental Effects Branch Thermal Vacuum Chamber (TVC) in support of the SLS Green Run tests[1]. Cork combustion was also observed during Titan IV Stage TPS testing[6]. Active burning of the base heat shield TPS contributed to the extensive charring as shown in Figure 3. It was not anticipated that the foil (covering the P50 cork to minimize radiative heating during Green Run) would liberate and that the base TPS fire intrusion would delaminate large acreage of foil and extensively char the TPS. As predicted from the pre-flight models[4,6], this large-scale combustion process was also observed on the foil-

less base heat shield during Artemis I flight from ~T+10 seconds to ~T+75 seconds[2-3]. This is based on flight instrumentation data and indirect inference of the phenomena. Visual imagery of SLS ascent base region terminated at T+43 sec. Based on Artemis I post-flight reconstruction, this regime led to the largest convective heating environments on the vehicle as predicted by the pre-flight models[4,6]. It was concluded that P50 cork combustion led to a large deflagration along the full acreage of the base with (Green Run) or without (Artemis I flight) the foil covering[1-2] as shown in Figure 2.

The primary objective of this paper was to characterize and understand the P50 cork combustion dynamics and the associated TPS material response during SLS ascent. The focus of this investigation was to understand the cork char response due to the various sensitivities in environments. This would lead to the enabling of more accurate TPS response due to base environments prior to Artemis II, the first crewed Artemis flight to the moon. Although the Core Stage Green Run[1] static hot-fire test campaign, completed at the B-2 test stand at Stennis Space Center, first provided a glimpse of these cork combustion environments on the base heat shield and aft end (Figures 2 and 3), various dynamics of this combustion process were largely unexplored. The characterization was done by ground testing completed at the NASA MSFC's TVC[9]. During Artemis I flight, the base heat shield TPS performance could not be used to provide substantiating data, as it was not instrumented with backside, or substrate thermocouples. Internal RS-25 thermocouples were the only means to determine intercompartment temperatures. However, controlled ground tests gave means to simulate the pressure-altitude and induced heat flux leading to the combustion phenomena and substantiating thermal data to further assess TPS performance.. Through ground and airborne imagery assets that track the flight path, the goal was to assess the ability to remotely measure TPS surface temperature with sufficient accuracy to be useful[4].

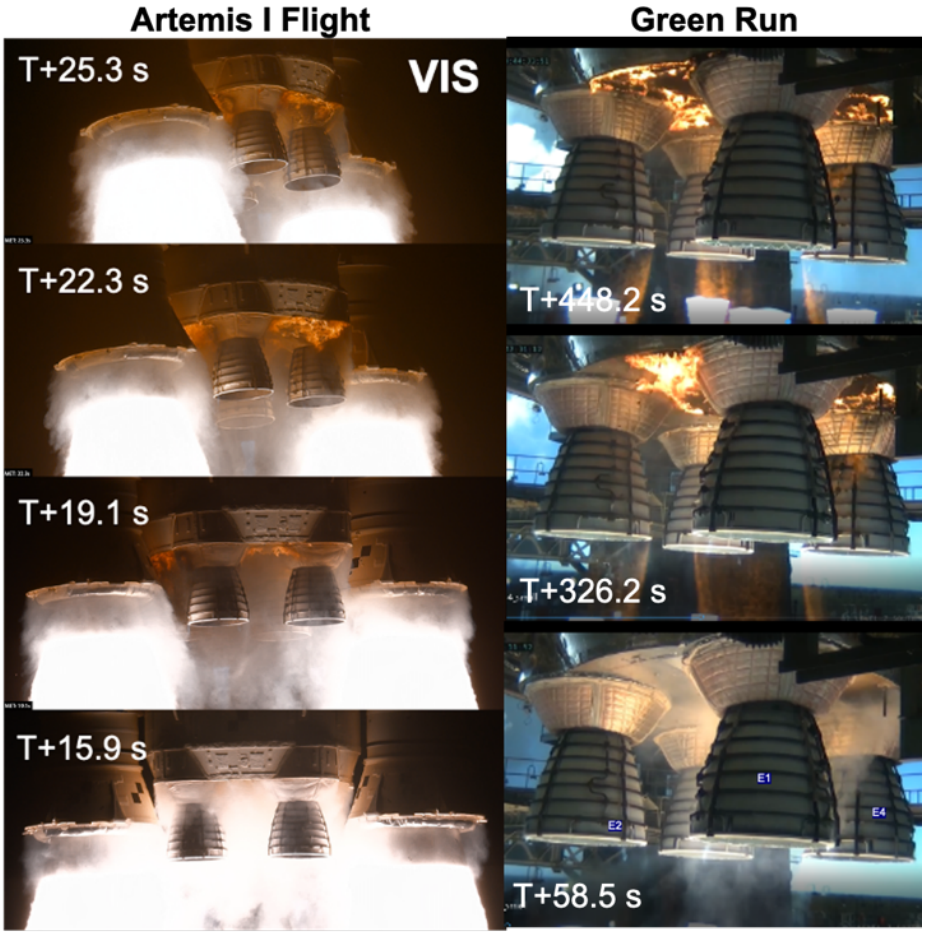

Figure 2. Artemis I (left) and Green Run (right) SLS Core Stage base heat shield TPS cork combustion phenomena[1-3].

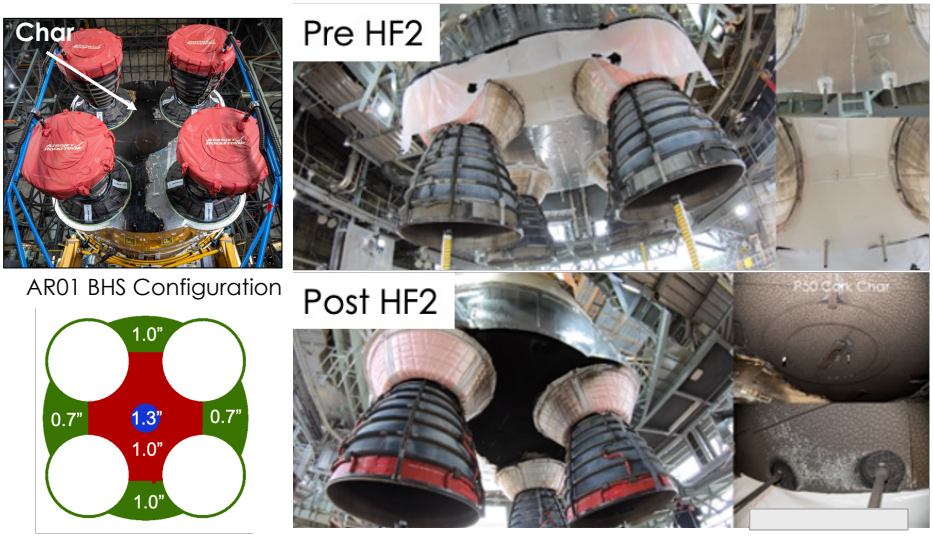

Figure 3. Extensive charring of the Green Run SLS Core Stage base heat shield TPS[1].

II. Methodology

A. Hot Gas Facility (HGF) Testing

The P50 cork char shear and heating recession characterization was conducted at the NASA MSFC Hot Gas Facility (HGF). HGF is an air – gaseous hydrogen combustion-driven wind tunnel capable of providing convective heating rates between 2 BTU/ft^2-sec (BFS) and 100+ BFS. It also has a radiant arc lamp that can output 15 BFS radiant heating. The HGF can provide both convective and radiative heating sources to the TPS samples. It typically is run at a Mach number of 4 based on the fixed diffuser area ratio as shown in the schematic below (Figure 4). The TPS sample was placed at the end of the expansion nozzle within the test section as shown in Figures 4 and 5. This facility has characterized many launch vehicle ascent TPS types in support of the Shuttle Program, Commercial Crew Program (CCP) and SLS Program.

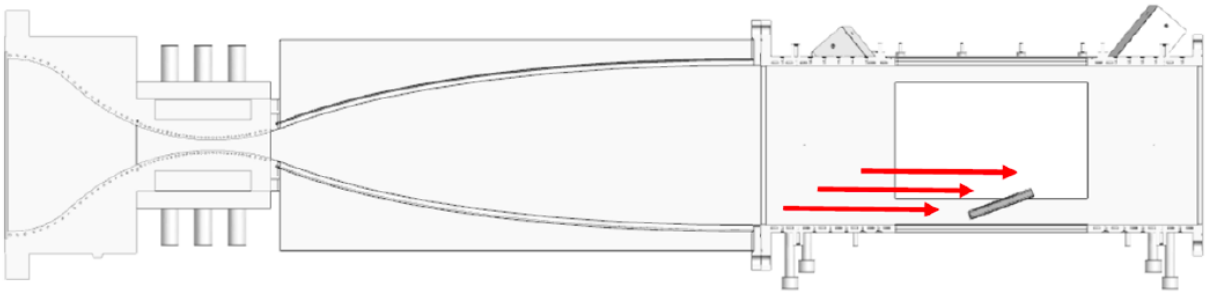

Figure 4. Schematic of TPS sample testing at the Hot Gas Facility.

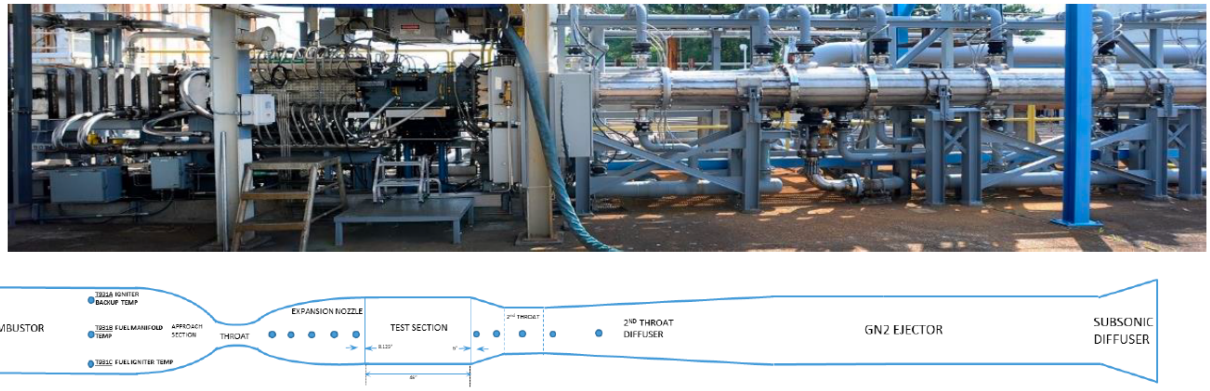

Figure 5. Photograph of the entire Hot Gas Facility (top); schematic of Hot Gas Facility wind tunnel components (bottom).

Figure 6 shows the placement of a HGF calibration plate and TPS sample within the test section. The sample and calibration plate were placed on a wedge to augment the convective heating rates. The calibration plate was used to ensure that the target conditions were satisfied in both convective heating, radiant heating, pressure and shear stress. Once the target conditions were met based on the appropriate wind tunnel mixing ratio, radiant arc lamp output, TPS placement wedge angle and chamber pressure, this condition was replicated with the TPS sample.

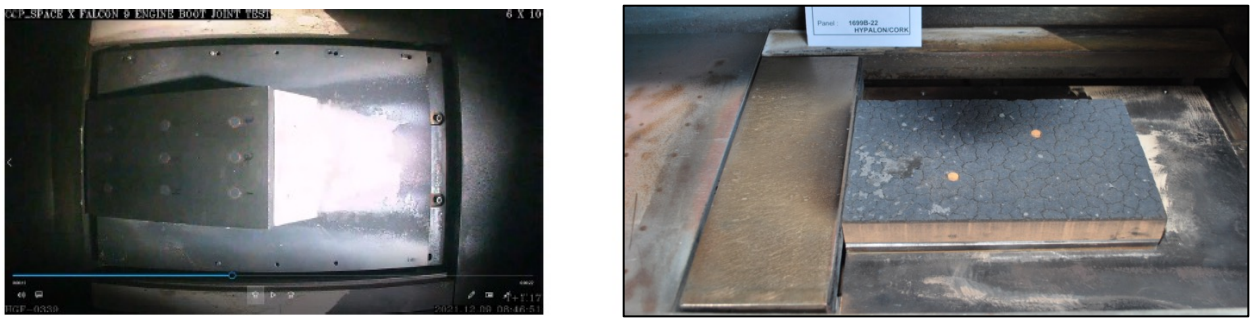

Figure 6. HGF calibration plate (left); TPS cork sample in the HGF (right).

B. Test Instrumentation

The calibration plate contained many different test sensors to quantify the environment levels induced by the flow field. The focus for this facility was launch vehicle ascent environments which targets the convective heating, radiant heating and wall shear stress. These were all drivers for TPS recession. The convective heating and radiant heating measurements were obtained using MEDTHERM[7] Schmidt-Boelter calorimeters and MEDTHERM Gardon radiometers. Shear stress measurements were obtained using the CUBRC Ahmic Aerospace shear stress gauges[8] as shown with a schematic in Figure 7. Below in Figure 7 is a layout for the 6” x 10” calibration plate that contained 5 calorimeters, 4 shear stress gauges and 6 pressure transducers.

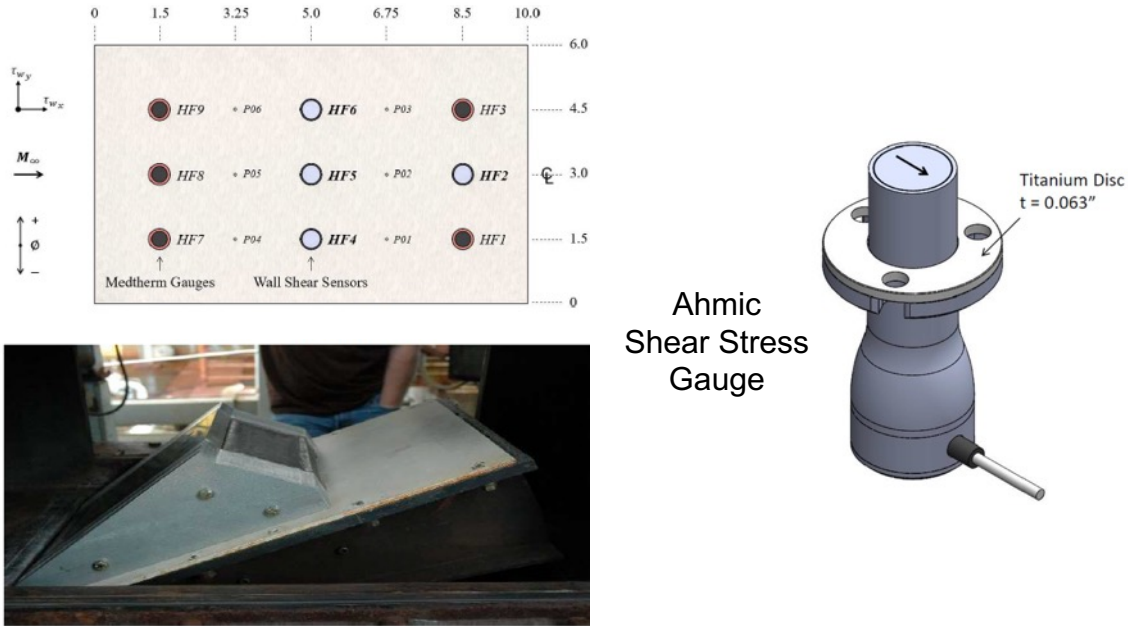

Figure 7. HGF calibration 6" x 10" plate which contains pressure transducers, heat flux sensors and shear stress gauges (top left); photo of calibration plate in the HGF (bottom left); schematic of Ahmic shear stress sensor (right).

C. Thermal Protection System Samples

The TPS samples that were characterized were uncoated and Hypalon coated P50 cork panels. Below is the TPS stack-up for the SLS Core Stage base heat shield and the NASA MSFC Nonmetallic Materials and Space Environmental Effects Branch's thermal vacuum chamber/HGF ground test campaigns. It was seen in Figure 8 that the stack-up for the ground test were similar to flight in material type and approximate in thickness. Figure 8 shows pictures of the calibration plate, P50 cork panel and Hypalon-coated P50 cork panel. The embedded calorimeter and radiometer were removed for the HGF TPS samples since only ablation and char erosion were being characterized.

There were two embedded TPS sensors that were removed for the HGF testing. This was the TPS embedded calorimeter (labeled TPS Cal), and embedded radiometer (labeled TPS Rad) as shown in Figure 8. This provided in-situ heating environments during test operations within the thermal vacuum chamber[9]. This instrumentation data is not described in this investigation as none of this data was collected for this test series.

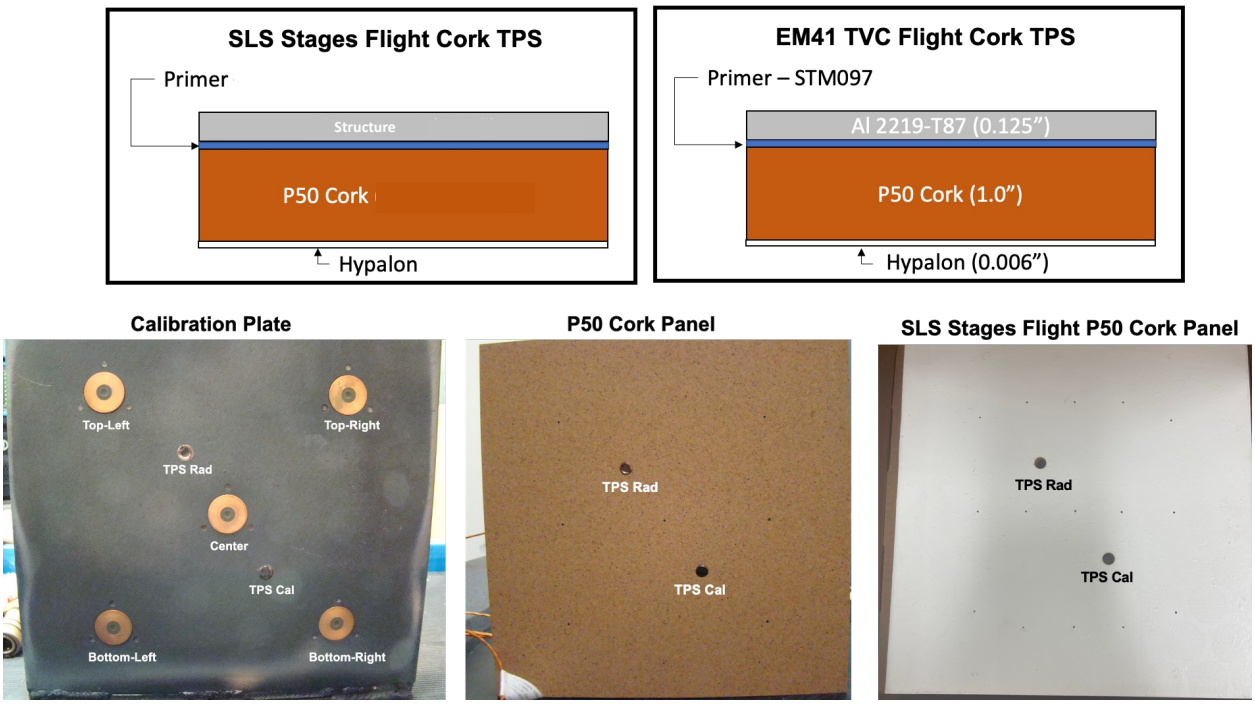

Figure 8. Comparisons of the TVC radiative heating TPS sample material stack-up and SLS Core Stage base heat shield TPS stack-up (top); TVC calibration plate (bottom left), P50 cork panel (bottom middle) and Hypalon coated P50 cork panel (bottom right).

The SLS Core Stage base contains Hypalon-coated P50 cork as the main ablator TPS. The largest acreage of this TPS was on the base heat shield and boattail, which are both important parts of the Core Stage base region. It was also found extensively on the barrel engine section and intertank (Figure 9). P50 cork has been installed at the high thermal environment areas for Artemis II through Artemis IV. Cork is also used as an ablator TPS on other elements of the SLS and Orion vehicles such as the solid rocket boosters and the launch abort system (LAS).

Prior to the HGF test campaign, most of the Hypalon-coated and non-coated P50 cork panels were subjected to radiant heating leading to cork combustion phenomena within the MSFC thermal vacuum chamber (TVC)[9]. These thermal environments resulted in a char layer of less than 0.2 inches for all these samples as shown in Figure 10. The top-down view of the TPS sample shows that the TPS was extensively charred and the Hypalon coating had partially been stripped away. After X-Ray computed tomography (CT) following the TVC testing[9], these samples were then delivered to the HGF for further characterization testing.

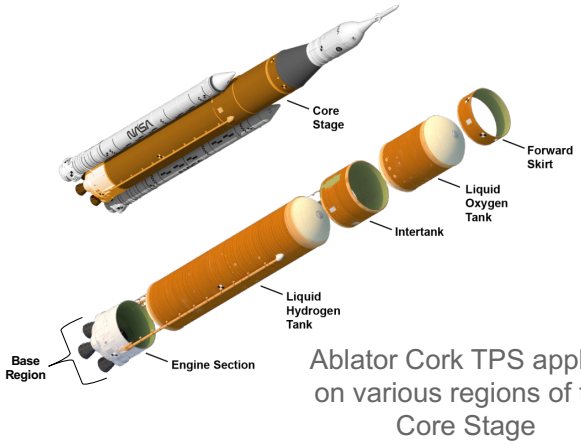

Figure 9. SLS Core Stage layout.

Figure 10. Pre-HGF test Hypalon P50 cork panel sample side profile (top) and top-down view (bottom).

D. Modified Hot Gas Facility (HGF) Test Matrix

Table 1 shows the test matrix for the HGF P50 cork char shear and heating characterization test campaign. The test campaign varied the total heating rate (dominated by radiant heating) from -1 BFS to 14 BFS and the shear stress varied from 0.4 pounds-per-square-foot (psf) to 2.0 psf. These heating rates and shear stress values were representative of launch vehicle ascent environments. The combustion-driven wind tunnel operated in a blow-down mode which varied the Mach number from Mach 0.1 to Mach 0.8. Two TPS samples were used: (1) Hypalon-coated P50 cork and (2) non-coated P50 cork. This test operation was an innovative approach in modifying the facility to gather important ground test data. All the TPS samples prior to HGF testing had a layer of cork char due to the cork combustion dynamics that occurred during the TVC test campaign[9]. The HGF test series was conducted to assess the cork char structural integrity due to flight environments.

Historically, HGF Mach 4 combustion-driven wind tunnel produced conservatively high shear stress for a given heating rate represented in flight. Wall shear stress values were in the range of 1 psf to 10+ psf that had been measured for typical convective heating rates observed for launch vehicles. This was about an order of magnitude higher shear than for typical flight ascent environments. These high shear stress contours on the TPS samples led to a conservative assessment of TPS recession for two reasons: (1) high shear extensively ablates and erodes the P50 cork char layer and (2) high shear led to removal of the pyrolytic gas insulating layer, leading to a higher thermal gradient and sustained heating, which increases the char layer. Both mechanisms provided a positive-feedback loop which increased the char layer thickness and recession. Minimal shear stress on the TPS would lead to increases in the insulating char layer, reducing the heat transfer toward the substrate material.

Table 1. HGF Test Matrix.

Modified HGF Test Conditions

Test Run	Total Heat Rate (BFS)	Air Mach Number	Test Duration (sec)	TPS Sample	Arc Lamp (On/Off)	Mean Shear Stress (psf)	Hi-Level Observations
R01	11.9	0.8	40	1699B-11 (P50 Cork)	On	1.70	All initial cork combustion char removed by shear loads
R02	11.9	0.8	40	1699B-21 (Hypalon/Cork)	On	1.70	Most of the char has been eroded
R03	12.3	0.6	40	1699B-22 (Hypalon/Cork)	On	1.20	Most of the char has been eroded
R04	13.9	0.1	40	1699B-20 (Hypalon/Cork)	On	0.5	Most of the char has been eroded
R05	-0.2	0.1	40	1699B-14 (P50 Cork)	Off	0.5	Minimal erosion of char
R06	-1.2	0.8	40	1699B-02 (P50 Cork)	Off	1.70	Minimal erosion of char
R07	4.9	0.1	40	1699B-13 (P50 Cork)	On	0.5	Splotchy spatial erosion of char
R08	12.3	0.6	40	1699B-09 (P50 Cork)	On	1.20	All initial cork combustion char removed by shear loads
R09	2.9	0.8	40	1699B-07 (P50 Cork)	On	1.70	

All TPS samples had a layer of P50 cork char prior to HGF testing due to high thermal environments induced by cork combustion dynamics

III. Development of Test and Artemis I Flight Base Shear and Heating Environments

A. Flight-Data Derived Calculations to Base Heat Shield Wall Shear Stress

The Artemis I SLS Core Stage did not have any flight shear stress gauges on the base heat shield, and to the author's awareness this type of instrumentation has never been included on any launch vehicle. As a result, a simplified launch vehicle base flow entrainment and recirculation model was developed to determine the gross wall shear stress on the Core Stage base heat shield during ascent. The McAnelly Aspirating Model[10-12] was used to determine the base flow Mach number from development flight instrumentation (DFI) on the base heat shield as shown with Equation 1 to Equation 5. This is also depicted as a schematic in Figure 11. Equation 1 defines the isentropic equations for base flow. The two main assumptions were that this process is adiabatic and reversible. Equation 2 defines the air entrainment model and Equation 5 defines the plume recirculation model. The air entrainment model suggested that the flow gets entrained from the freestream outside of the boattail toward the center of the base heat shield due to an ejector effect from the four RS-25 engine plumes and two SRB motor plumes. The rocket nozzle exit Mach number of these plumes was on the order of Mach 4 and the plume shear layer can effectively entrain the surrounding medium. This model did not capture the small, localized recirculation zones at the boat-tail periphery and more pronounced recirculation along the SRB-line observed through computational simulations, but the gross flow field observations were supported by the McAnelly Aspirating Model[10-12]. This was a result of the low spatial resolution of pressure sensors along the base heat shield. This net flow field during the aspirating flow regime was observed during Green Run[1] and other sub-scale power-on wind tunnel tests using base pressure transducers[4], smoke flow (Figure 11) and surface oil flow visualization techniques[10-12]. Similar models were developed during the Saturn program and were used to assess base flow characteristics[10-14].

Similar to the aspirating flow model, the plume recirculation model was observed by many flow visualization techniques[10-13] (Figure 11) and computational simulations where the plume jet stagnates at the base center and propagates towards the periphery. This occurred when the multi-engine plumes were highly under-expanded and developed Type 1 Edney shock interactions, leading to high enthalpy nozzle boundary layer gas propagating forward

towards the base heat shield central region. During the choked flow regime, the mass flow rate of the plume gas flowing outward from the center to the base periphery is constant. The choked flow regime led to a relatively constant base flow Mach number (Figure 12). This occurred around T+150 sec during the Artemis I flight[2-3]. Peak recirculation showed the highest base flow Mach number acceleration from the base center to the periphery.

Figure 12 shows a comparison of the average base vent flow Mach number along the Core Stage base heat shield during Green Run Hot-Fire 2, and Artemis I flight[1-2]. There was a significant difference between the base flow Mach number between the two conditions. During the static test fire of the four RS-25 engines at NASA Stennis B-2 test stand, there was only aspiration of the freestream toward the center of the base. The entrained base air flow Mach number was calculated from the aspiration model to be between Mach 0.03 and Mach 0.07. This was observed from three flight measurements along the Core Stage base periphery as shown in Figure 12 (left panel). During Artemis I flight, the Core Stage base flow went through multiple flow regimes such as aspiration, transition, peak recirculation and choked flow. The transition flow regime occurred when the freestream entrained flow was balanced by the initial plume-plume interaction recirculated flow, leading to a base pressure differential ($P_b - P_{inf}$) of zero[2-3]. There was a local minimum during base flow transition as observed in Figure 12 (right panel). Peak recirculation led to the highest base flow Mach number which accelerated above Mach 1. As expected, the freestream Mach number (shown in blue in Figure 12, right panel) was much higher than base vent flow velocities. The choked flow regime had base flow gases accelerating at an average of Mach 1. This average base flow velocity was calculated between the RS-25 engines near the periphery of the base heat shield (usually termed as the vent exit regions) where sensors were collocated. Figure 12 shows that the flight regime exhibited approximately two orders of magnitude higher base vent flow velocities than during the static Green Run test. The region highlighted in red in Figure 12 denotes the base heat shield P50 cork combustion regime during Artemis I[2-3]. During the Green Run, depending on the base location, deflagration of the heat shield was observed from T+100 sec to RS-25 engine shutdown (~T+500 sec)[1].

Equations 6 – 12 show the derivation of the base wall shear stress from all the DFI on the base heat shield. The wall shear stress was derived from the classic Reynolds-Colburn Theory[15] as shown in Equation 6. The Reynolds-Colburn theory shows the relationship between momentum transfer and energy transfer to be approximated by the standard *Nu-Re-Pr* correlations[15]. This was based on a few assumptions where a fully turbulent flow developed, and the Prandtl number of the gas was near unity[15]. This model also assumed that the normal pressure gradients were small. The base flow velocity was calculated from Equation 7 which was grounded by pressure measurements and the base flow heat transfer coefficient was obtained from Equation 8. The heat transfer coefficient was entirely derived from DFI measurements. The aspirating base flow thermal conductivity and gas viscosity were based on Sutherland's Law of Transport Properties[15] of air which was function of the static temperature. The plume gas transport properties during the recirculating flow and choked flow regimes were calculated from the Chemical Equilibrium Code[16] (CEC) with known inputs of gas pressure and temperature. Equation 10 derives the static temperature from the gas temperature probe (GTP) measurements and base flow Mach number. Base flow wall shear stress was a function of the gas transport properties, heat transfer coefficient and base flow velocity (Equation 11).

Similar to comparisons with base vent flow Mach number, Figure 13 shows the base heat shield wall shear stress vs. time between the Green Run static fire test and Artemis I flight at the three DFI island locations[1-3]. The base flight shear stress loads are broken into three regimes: (1) cork combustion; (2) peak recirculation; (3) choke flow. More than two-orders of magnitude higher average shear stress were observed during flight as compared to the static-fire test series. This was because the convective base heating and flow velocities were substantially higher for flight than Green Run. This large difference in shear stress for flight has an impact on TPS recession and performance and provided rationale to investigate cork TPS response to flight environments.

Figure 14 shows the base heat shield wall shear stress at the four locations where substantial DFI measurements were made during flight[1-3]. The four locations are between the RS-25 engines near the periphery of the base heat shield. It shows the four main phenomena[1-3] that occurred during Artemis I: (1) P50 cork combustion; (2) peak recirculation; (3) SRB shut-down spike and (4) choked flow. The shut-down spike occurs when the SRB thrust trails-off and develops solid-liquid aluminum-oxide slag exiting the booster nozzles. It should be noted that the flow field composition was more difficult to adequately predict during the shut-down spike and as such there was significant uncertainty in the wall shear stress prediction during this period. The shutdown-spike occurred during Artemis I flight from an altitude of ~140,000 ft to 175,000 ft (Figure 15). Peak recirculation shows the largest wall shear stress on the order of less than 1.5 psf at an altitude of 105,000 ft. The choked flow regime showed the derived wall shear stress values ranging from 0.2 psf to 0.6 psf, resulting from the low gas pressure and density during this period of flight.

Wall shear stress estimates near the DFI sensor TOT034 showed large data scatter during the Core Stage only burn (Figure 14). There is more variability in the shear stress during the aspirating and P50 cork combustion regimes, but the average wall shear stress is on the order of 0.2 psf with peak values of 1.0 psf. The shear stress in the aspirating flow regime can incur higher uncertainty due to model assumptions.

Figure 15 shows comparisons between flight data derived methodologies of wall shear stress with computational fluid dynamics (CFD) simulations (shown as black and white dots in the figure) as a function of altitude. These steady-state simulations were conducted using smooth-wall Reynolds-Average Navier Stokes (RANS) turbulence modeling. Two CFD data points were provided: (1) mean wall shear distribution in the general DFI zonal location shown as black dots; (2) peak wall shear stress values in the general DFI zonal location shown as white dots. There was generally good agreement between the CFD simulations and the flight data-derived calculations. CFD simulations slightly underpredicted the flight data derived calculations during aspiration, P50 cork combustion and recirculation regimes, but showed very good agreement during the choked flow regime. It should be noted that a rough TPS wall caused by ablation will induce higher shear stress. It can be seen from both CFD and flight data derived calculations that the flight base wall shear stress could vary between 0.2 psf and 1.5 psf across the full flight regime. This was an important metric in conducting a ground test that investigated the effect of char recession due to flight shear environments. All the RANS CFD calculations were performed by M. Elizabeth Arceneaux and Dr. Francisco Canabal of the MSFC Aerosciences Branch.

With the assistance of the Michoud Assembly Facility, the ground test TPS panels were made similar in configuration and thickness to the flight SLS system (Figure 16). The standard material stackup was a primer that adhered the P50 cork to the aluminum substrate. The P50 cork, which is the main ablator, was then coated with Hypalon paint to minimize water absorption into the porous TPS which could change the thermal performance. Figure 16 also shows the various thicknesses of cork TPS across the Core Stage base heat shield for Artemis I. These thicknesses had been increased before flight to account for the possibility of cork combustion[1]. During flight, the cork TPS on the base heat shield did indeed experience combustion for approximately 60 seconds in the high radiative heating environment, as shown in Figure 17. To be consistent, all the TPS cork panels used in the HGF were subjected to cork combustion phenomena in the TVC and generated a char layer of less than 0.2 inch in thickness[9]. Figure 17 shows that the TVC ground test adequately replicated the TPS combustion phenomena observed in flight[1,9]. The goal of this investigation was to understand the mechanical erosion and ablation of P50 cork char due to flight shear and heating environments.

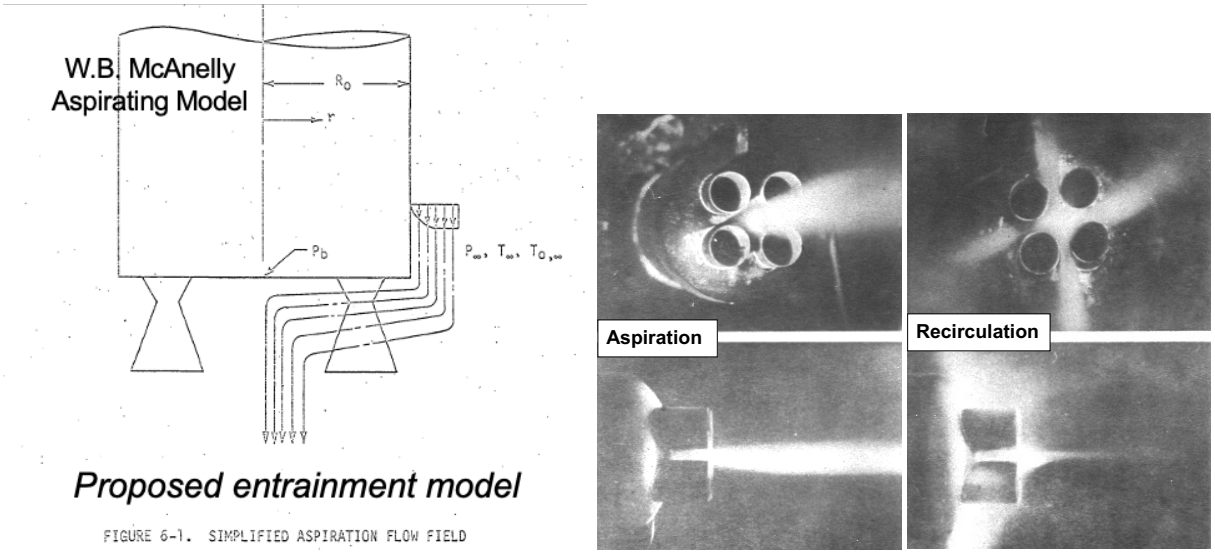

Figure 11. Schematic of the W.B. McAnelly simplified launch vehicle base aspiration flow field model[8-11] (left); smoke flow visualization of a power-on wind tunnel model during the aspiration and recirculation regimes (right)[10-11].

$$\frac{P_0}{P} = \left(\frac{\rho_0}{\rho}\right)^{\gamma} = \left(\frac{T_0}{T}\right)^{\frac{\gamma}{\gamma-1}} \qquad (1)$$

$$Ma_{P033} = \sqrt{\frac{2}{\gamma_\infty - 1} r_{P033}^{\frac{\gamma_\infty - 1}{\gamma_\infty}} - 1} \qquad r_{P033} > 1 \qquad (2)$$

$$r_{P033} = \frac{P_\infty}{P_{P033}} \qquad (3)$$

$$r2_{P033} = \frac{P_{P027}}{P_{P033}} \qquad (4)$$

$$Ma_{P033} = \sqrt{\frac{2}{\gamma_p - 1} r2_{P033}^{\frac{\gamma_p - 1}{\gamma_p}} - 1} \qquad r_{P033} \leq 1 \qquad (5)$$

$$\frac{C_f}{2} = \frac{Nu}{RePr^{1/3}} \qquad (6)$$

$$U_j = Ma\sqrt{\gamma R T_s} \qquad (7)$$

$$h = \frac{\dot{q}_T^{\text{Cal}} - \dot{q}_R^{\text{Rad}}}{T_{rec}^{\text{GTP}} - T_w^{\text{Cal}}} \qquad (8)$$

$$k = f(T_s)$$
$$\mu = f(T_s) \qquad (9)$$

$$T_s = \frac{T_{rec}^{\text{GTP}} \xleftarrow{\text{Measurement}}}{(1) + \left(((\gamma - 1)/2) Ma^2\right)} \qquad (10)$$

$$\tau_w(H) = \frac{hU_j\mu}{kPr^{1/3}} \quad (11)$$

Wall Shear Stress; Jet Heat Transfer Coefficient; Jet Velocity; Jet Viscosity; Jet conductivity

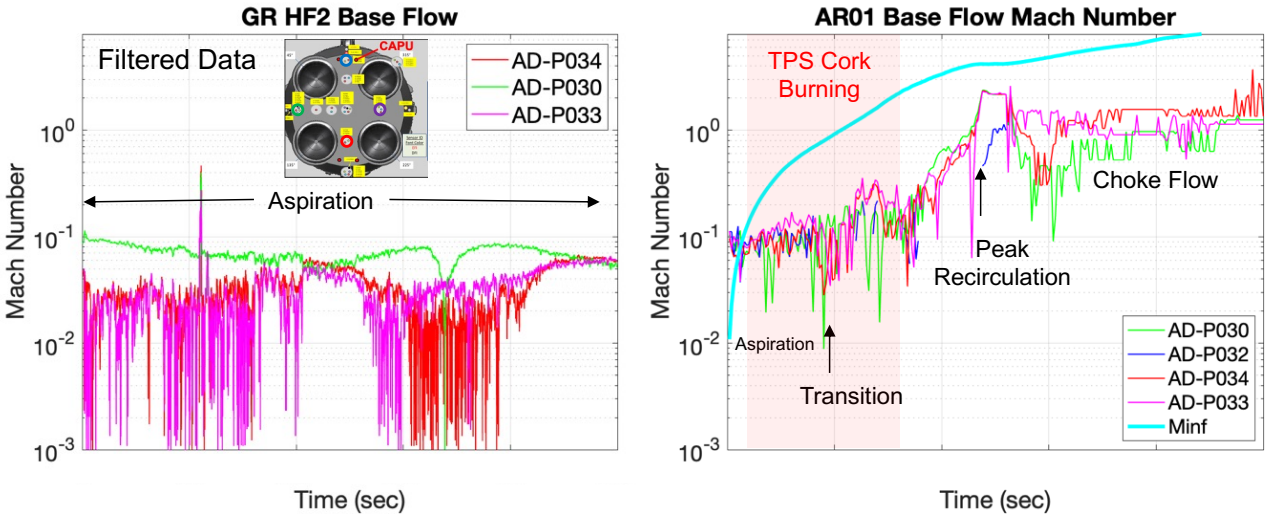

Figure 12. Base vent flow Mach number vs. time at various locations on the Core Stage base heat shield during Green Run Hot-Fire 2 (left) and Artemis I flight (right).

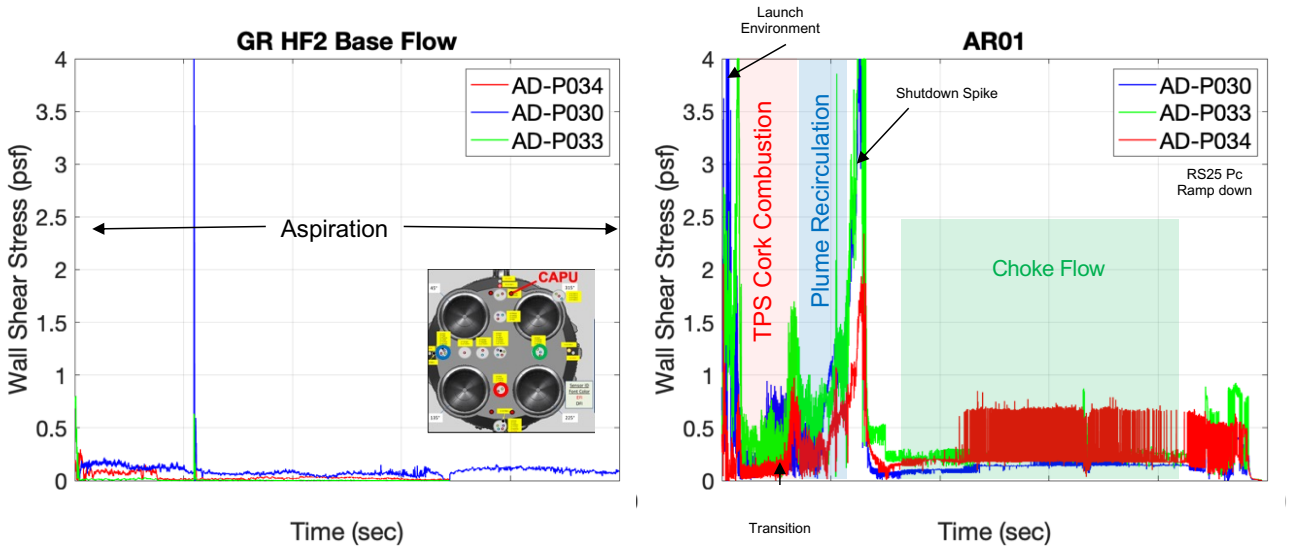

Figure 13. Base wall shear stress vs. time at various locations on the Core Stage base heat shield during Green Run Hot-Fire 2 (left) and Artemis I flight (right).

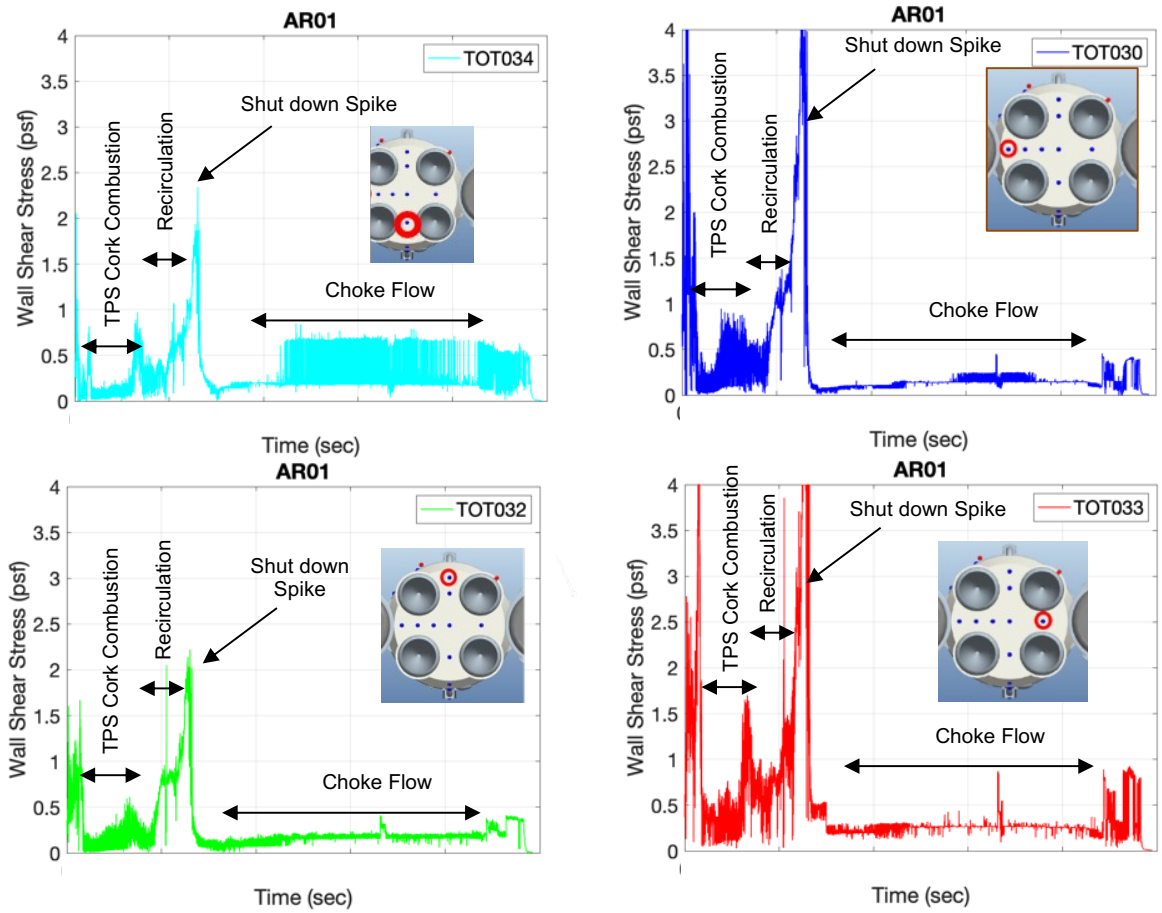

Figure 14. Base flow wall shear stress vs. time on the Core Stage base heat shield during Artemis I flight for the various flow regimes at the location between E2 and E3 (top-left); near left SRB (top-right); between E1 and E4 near CAPU exhaust (bottom-left) and near right SRB (bottom-right).

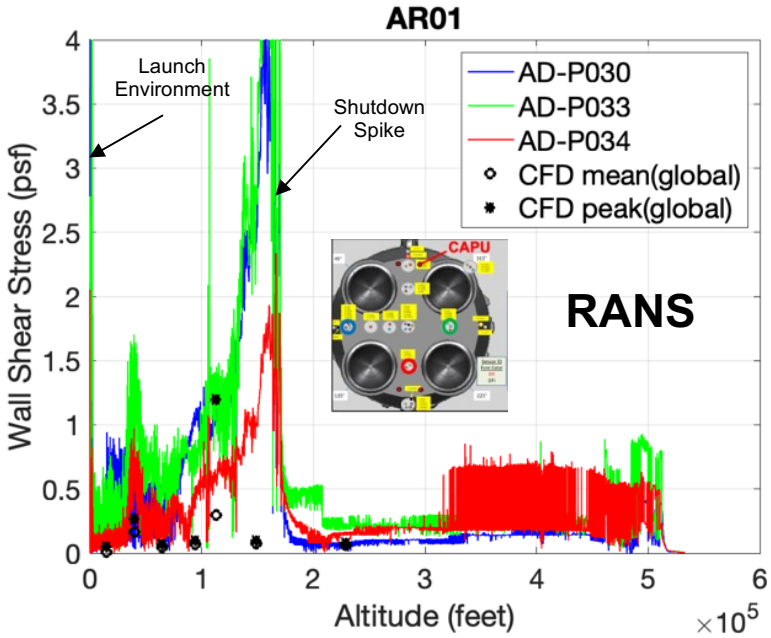

Figure 15. Base flow wall shear stress vs. altitude at various locations on the Core Stage base heat shield during Artemis I flight. Flight data derived estimates compared to CFD RANS solutions.

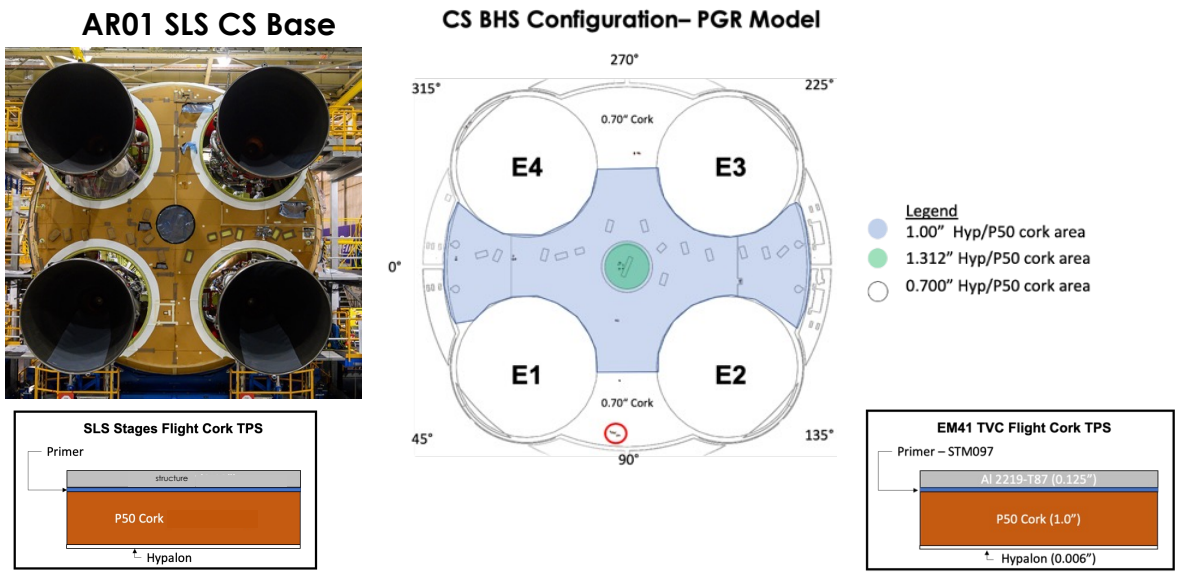

Figure 16. Photo and schematic of Artemis I Core Stage base heat shield TPS design and material stack-up.

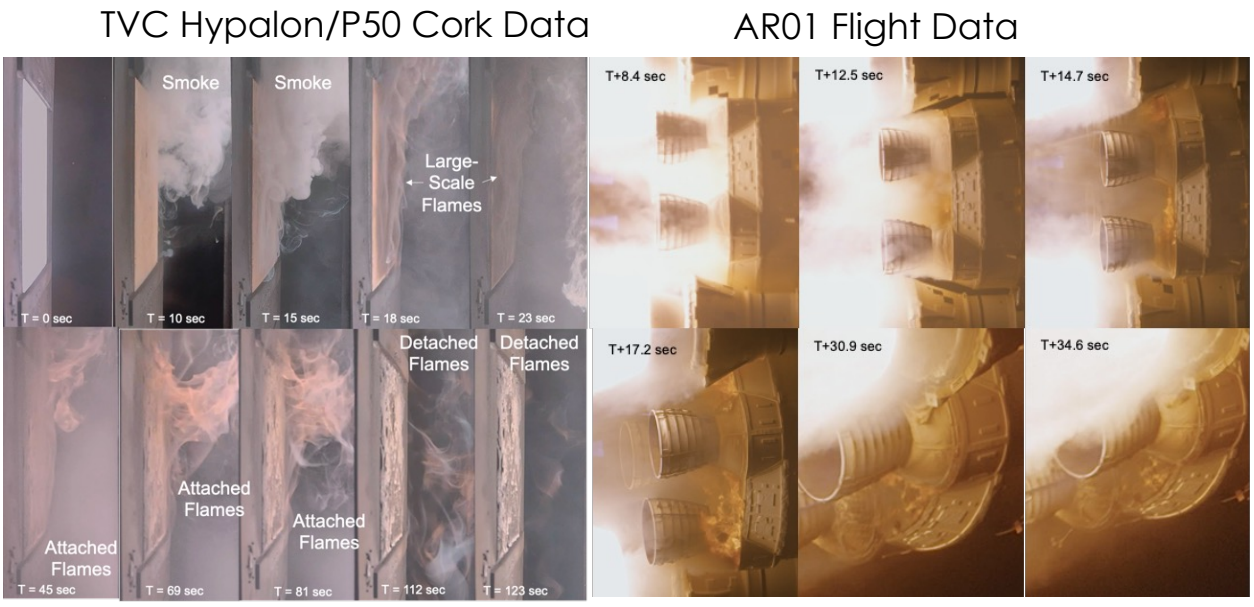

Figure 17. Time-evolution visible and IR imagery data of Hypalon-coated P50 cork combustion dynamics during TVC TPS panel testing (left) and Artemis I SLS Core Stage base heat shield (right)[2-3,9].

B. Heritage HGF vs. Modified HGF Operations and Environments

The heritage HGF operation produced Mach 4 high enthalpy flow conditions, resulting in shear stress measurements significantly higher than the estimated flight-representative values developed in Section III A (Figure 18). Figure 18 (left panel) shows a comparison of heritage HGF wall shear stress measurement (shown as red dots) with flight data derived calculations (shown as small black dots) for the whole Artemis I SLS flight regime. It can be seen that the wall shear stress measurements in the heritage HGF operational mode were significantly higher than the predicted values from flight. The high shear stresses likely lead to virgin and cork recession rates which are higher than what would be obtained using more flight-representative values. This is prudent for a conservative TPS design methodology but makes it challenging to assess the true performance of an ablator in a flight environment. Hence, a

modified operation of the HGF was used to assess char recession in a shear and heating environments more like flight. As can be seen in Figure 18 (right panel), the modified HGF shear stress and normalized heat transfer parameter measurements (magenta dots) were more in-family with flight environments (small green dots). The normalized heat transfer parameter is defined as a ratio of the total heat flux to a reference peak total heat flux for that location. This enabled assessment of the char recession effects to flight-like environments. This was the first time this mode of HGF operation was done to assess TPS char/virgin response.

Figure 19 shows the comparisons of the modified HGF shear and normalized heat transfer parameter with Artemis I flight environments at four DFI islands on the base heat shield. The four islands were located towards the periphery of the base heat shield and between the RS-25 engines[1-3]. Once again, good agreement between the modified HGF environments with flight environments was observed. This was the main goal behind the modified HGF testing. The total heating from the modified HGF was established with a combination of both radiant and convective heating contributions. It should be noted that majority of the heating to the sample was generated from a radiant arc lamp for the ground test. Both radiant and convective heating were major contributors of surface heat transfer during flight.

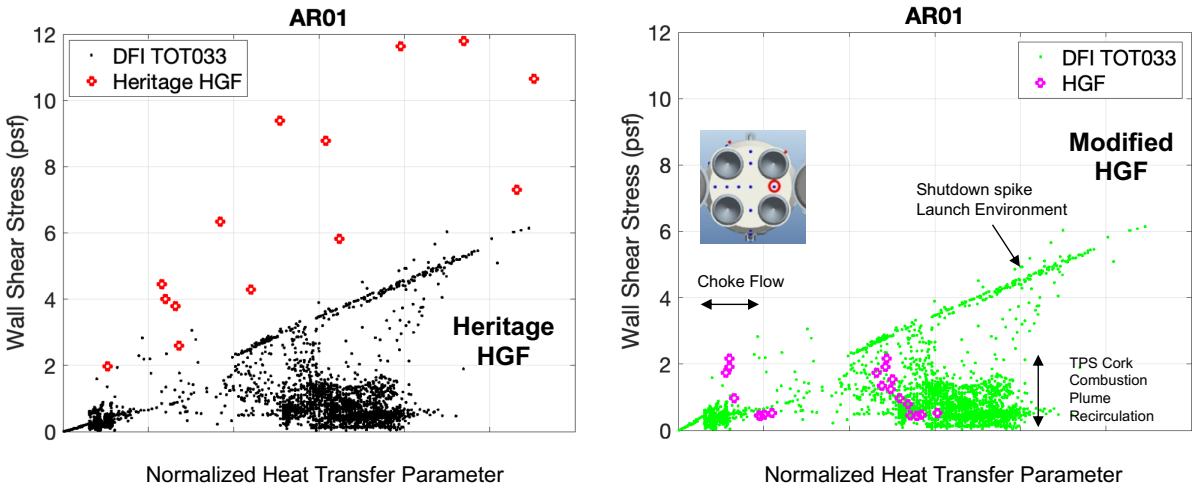

Figure 18. Comparisons of base flow wall shear stress vs. normalized heat transfer parameter at the RSRB facing Core Stage base heat shield during Artemis I flight with heritage operations of the Hot Gas Facility (left) and modified operation of the Hot Gas Facility (right).

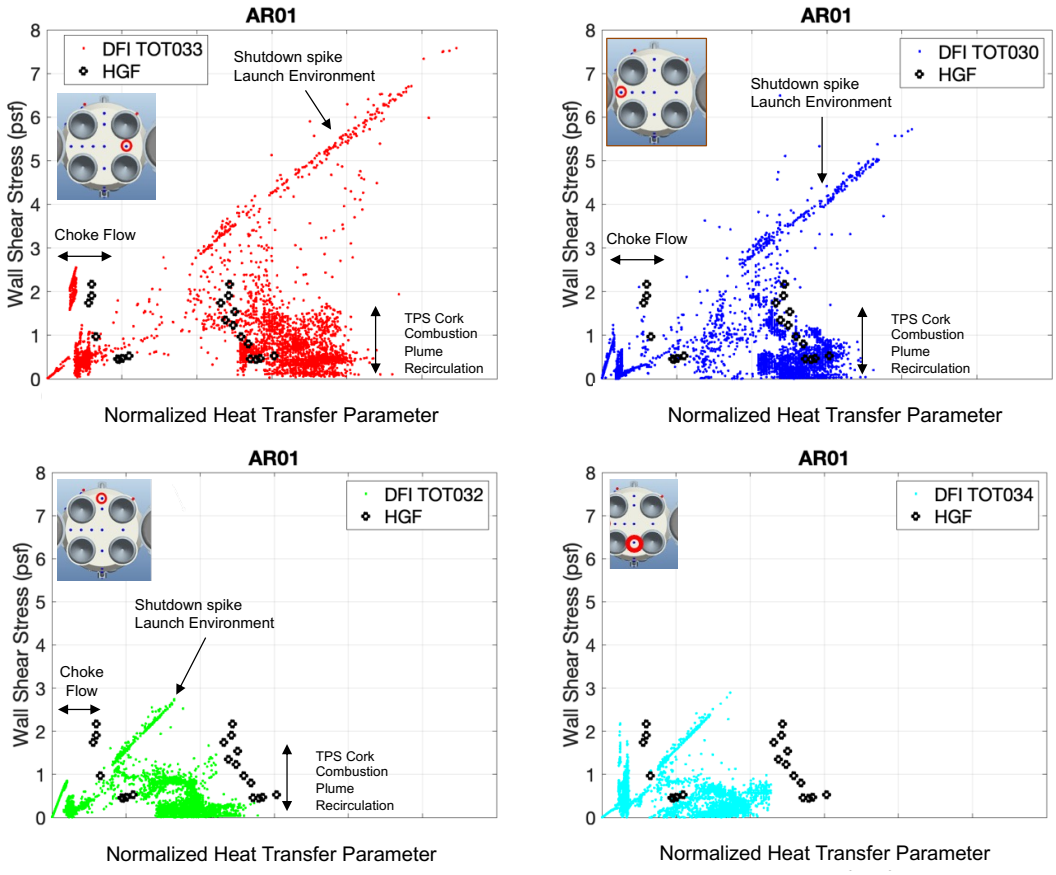

Figure 19. Comparisons of base flow wall shear stress vs. normalized heat transfer parameter at the various locations on Core Stage base heat shield during Artemis I flight with modified operation of the HGF. Right SRB facing (top-left); LSRB facing (top-right); between E1 and E4 near the CAPUs (bottom-right) and between E2 and E2 near CAPUs (bottom-right).

IV. Hot Gas Facility TPS Test Results

A. Pre-HGF and Post-HGF TPS Panel Imagery Data

A subset of pre-HGF and post-HGF TPS panel imagery data is shown below in Figures 20 – 22. The rest of the TPS panel imagery data sets are shown in Appendix A (Figures A2 and A3). The subset image data set show the gross differences of the TPS response due to changes in the heating and shear environments. An external side and top-down views of the TPS panels are shown in the figures. All pre-HGF TPS panels showed burning effects with a developed thick char layer from TVC testing[9] and Figure 20 shows the Hypalon paint burned and shredded apart with the char layer exposed. The char formed black honeycomb cells at the top surface layer based on the top-down view images. One notable observation between Figure 20 and Figure 22 showed that the high heating and shear environments substantially reduced the honeycomb cell diameter. This reduction in the char honeycomb cell diameter topology was a stronger function of the heating than shear stress based on findings from Figure 22 and Figure A2 (Run 2). The reduced char honeycomb cell observation (Figure 20) showed a smoother feature than the large char honeycomb cell diameter topology (Figure 22). Qualitatively it seemed that the shear stress in a high thermal environment uniformly eroded the char layer, and this was further supported by imagery data within Appendix A. Since one of the main objectives of this test series was to look at various sensitivities for TPS response, it was found that a threshold in TPS erosion/ablation was noted for Run 7 (Figure 21). The post-test TPS image showed regions of minimal char erosion/ablation and other areas of substantial erosion. Higher char erosion was noted along the leading edge of the TPS cork panel. There was no side view visible imagery data collected for Run 9 (Figure 22).

Average Total Heating = 13.9 BFS
Average Shear Stress = 0.5 psf

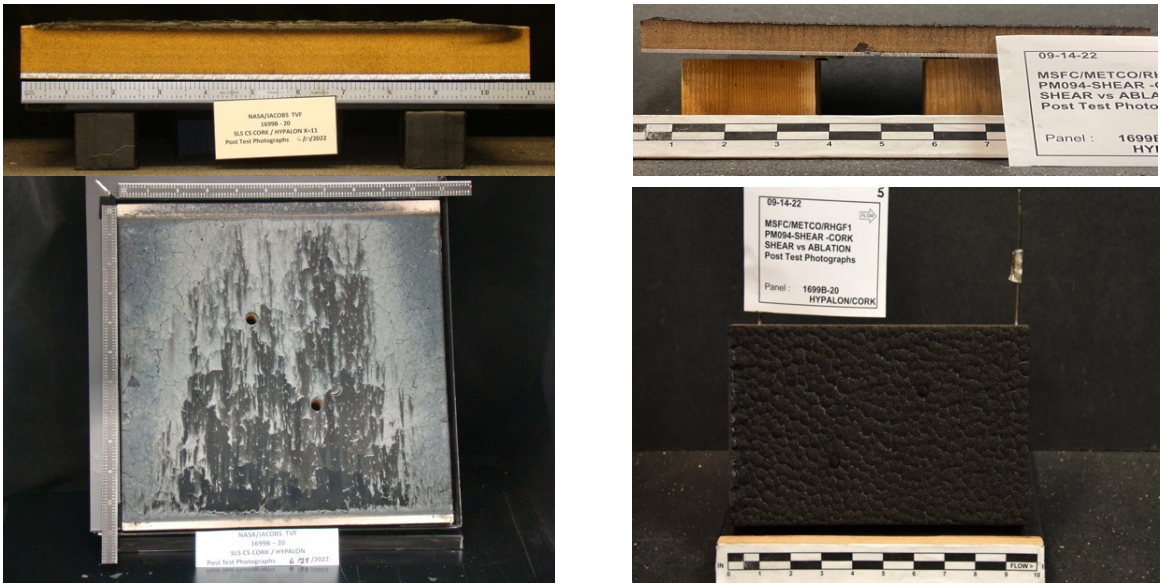

Figure 20. HGF Run 4: Pre-HGF test TPS sample top-down and side images (left) and post-HGF test TPS sample images (right).

Average Total Heating = 4.9 BFS
Average Shear Stress = 0.5 psf

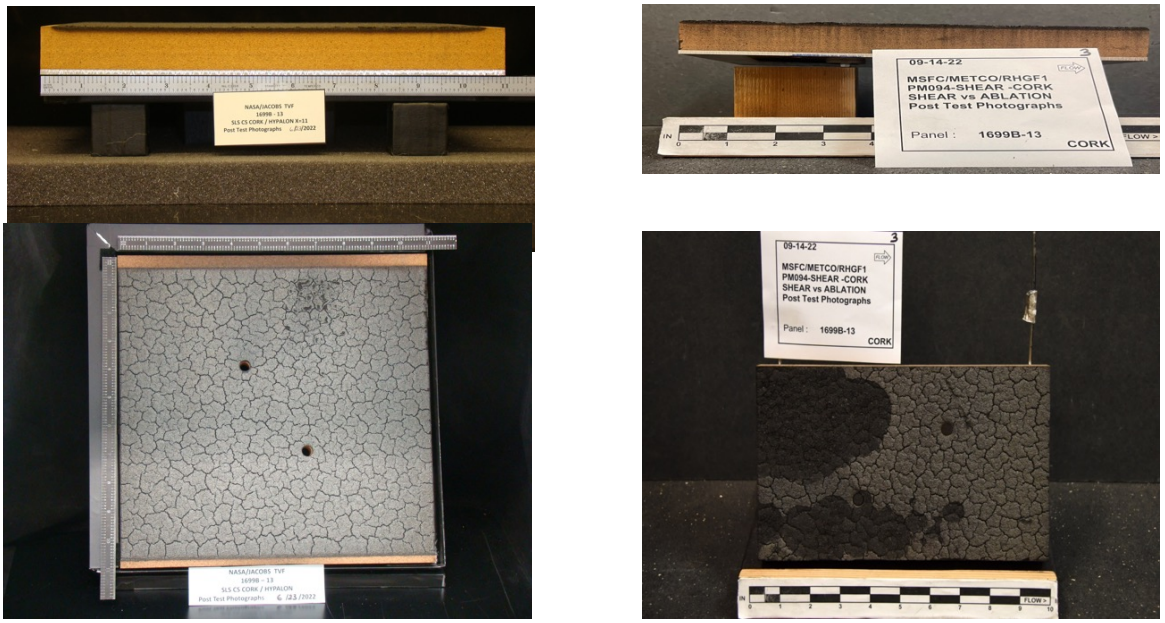

Figure 21. HGF Run 7: Pre-HGF test TPS sample top-down and side images (left) and post-HGF test TPS sample images (right).

Average Total Heating = 2.9 BFS
Average Shear Stress = 1.7 psf

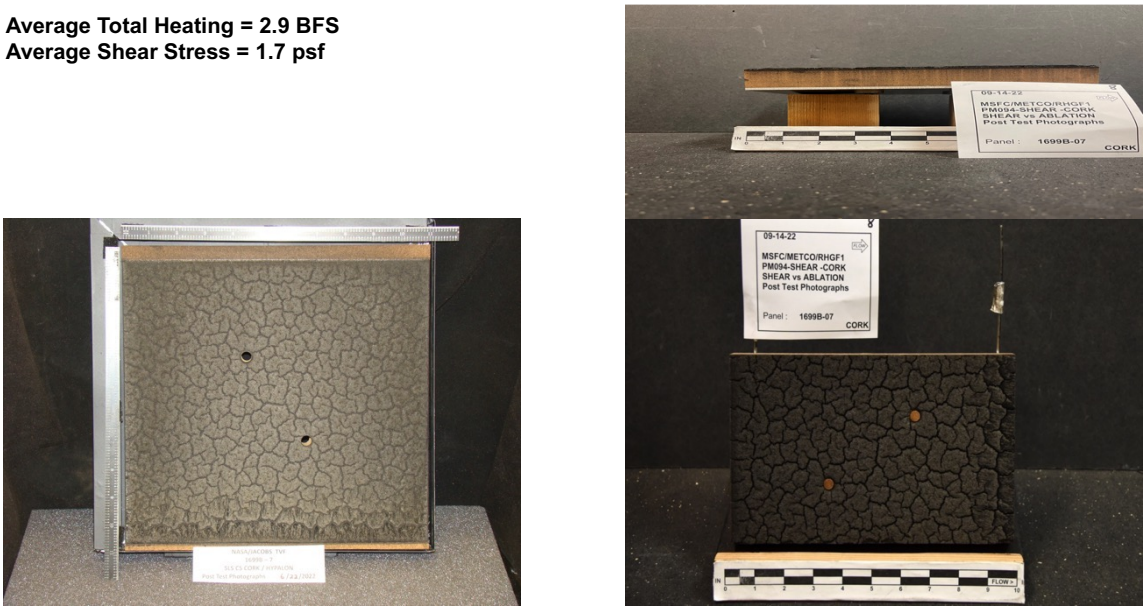

Figure 22. HGF Run 9: Pre-HGF test TPS sample top-down and side images (left) and post-HGF test TPS sample images (right).

B. X-Ray CT scans of Pre-HGF and Post-HGF TPS Panels

Figures 23 – 25 show X-Ray Computed Tomography (CT) scans bisected the internal regions of the TPS panel for different TPS panel environments. There were three large-scale features noted here, the aluminum substrate, cork virgin material and the cork char layer. It was seen that the aluminum substrate resulted in X-Ray back scatter which bled high intensity pixels into the cork virgin region. The char layer was much darker than the virgin layer due to a large reduction in the material density of the char. The top panels of each figure were the TPS X-Ray CT scan for pre-HGF testing and bottom panel of each figure was the TPS X-Ray CT scan for post-HGF testing. The two solid lines in the top panel refer to the char layer prior to HGF testing. The dashed lines on the bottom panel for each figure is the pre-HGF test char height. Figure 23 shows the char response due to minimal heating and high shear which showed that most of the char layer adhered to the pyrolytic zone and the char density was substantially larger. Figure 25 shows the char response due to high total heating and moderate shear which suggested that most of the char layer had been stripped cleanly from the pyrolytic zone. Figure 24 shows regions where the char had been eroded and other regions where the char stayed adhered to the pyrolytic zone. This case exposed the TPS panel to moderate total heating and shear stress. The pyrolysis zone could not adequately be captured with X-Ray CT for these samples and more refinement of the scanning and post-processing needed to occur to distinguish char from the pyrolysis zone.

Average Total Heating = 2.9 BFS
Average Shear Stress = 1.7 psf

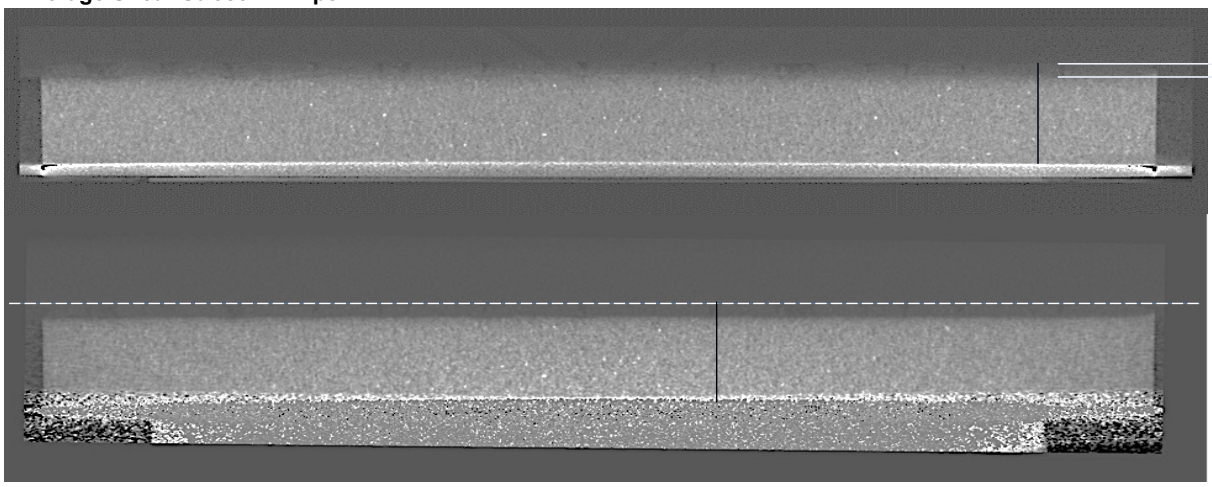

Figure 23. HGF Run 9: Pre-HGF test TPS sample side view X-Ray CT image (top); two white solid lines show char depth from P50 cork combustion process within the TVC (top) and post-HGF test TPS sample X-Ray CT image (bottom); dashed white line shows the initial top-surface of the pre-HGF test TPS (bottom).

Average Total Heating = 4.9 BFS
Average Shear Stress = 0.5 psf

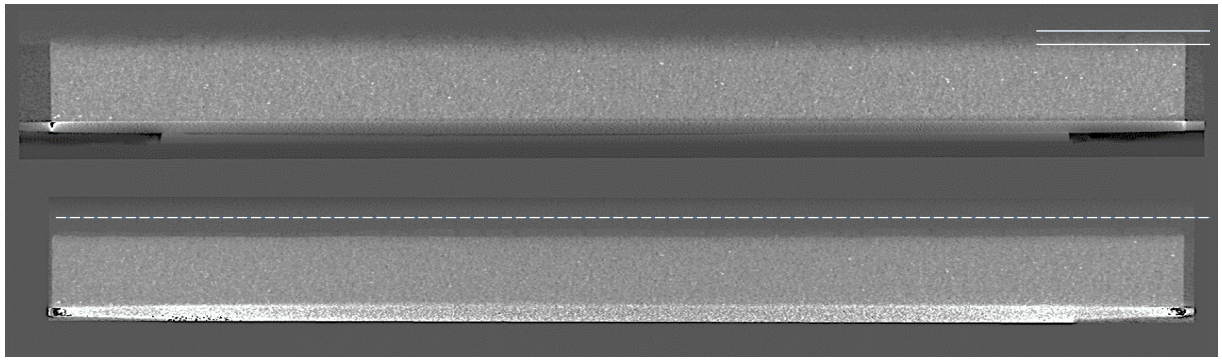

Figure 24. HGF Run 7: Pre-HGF test TPS sample side view X-Ray CT image (top); two white solid lines show char depth from P50 cork combustion process within the TVC (top) and post-HGF test TPS sample X-Ray CT image (bottom); dashed white line shows the initial top-surface of the pre-HGF test TPS (bottom).

Average Total Heating = 13.9 BFS
Average Shear Stress = 0.5 psf

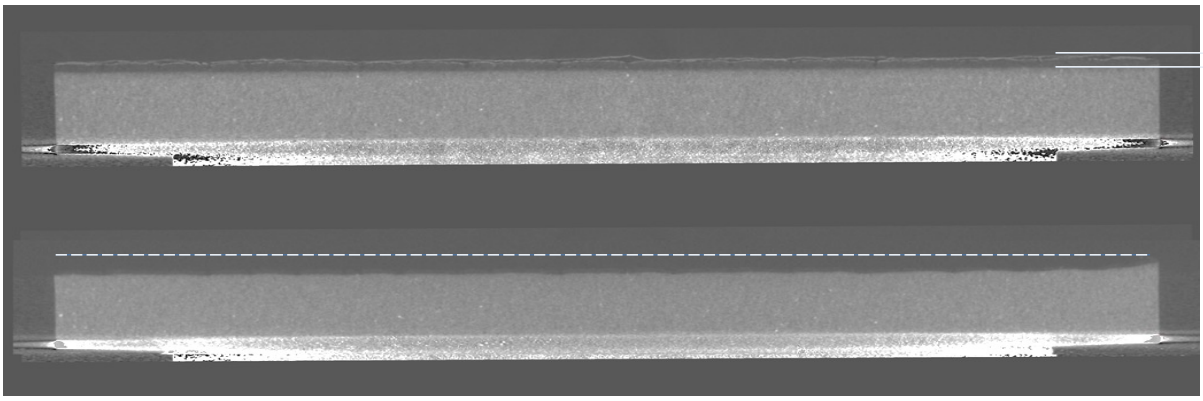

Figure 25. HGF Run 4: Pre-HGF test TPS sample side view X-Ray CT image (top); two white solid lines show char depth from P50 cork combustion process within the TVC (top) and post-HGF test TPS sample X-Ray CT image (bottom); dashed white line shows the initial top-surface of the pre-HGF test TPS (bottom).

V. Discussion and Analysis

Most of the following discussion and analysis will be centered around char recession sensitivities to total heat flux and wall shear stress. This paper is not investigating the virgin cork recession characteristics that have been done in the past, but rather cork char. To the author's awareness, cork TPS recession has never been directly measured in-situ in flight. The focus on char recession characteristics was due to the large-scale burning that occurred early in flight which would result in the development of the char layer. Cork combustion and peak recirculation led to further induced shear and thermal stress on the char layer of the base heat shield. One of the many goals was to assess cork char structural integrity due to flight environments. Since the heritage HGF operation produced almost an order of magnitude higher shear for a given heat flux, it was assumed that most of the char would quickly erode. However, it was not known how the char would behave in more benign flight shear environments and what the various thresholds might be to further characterize the char recession.

Figure 26 shows char recession rate measurements as a function of total heat flux measurements for 8 charred cork samples. It should be noted that B20, B21 and B22 (not shown) were Hypalon-coated P50 cork char TPS panels and the rest were with bare P50 cork. The char recession rate was calculated using X-Ray CT measurements of the top-surface of the TPS panel between pre-HGF and post-HGF testing. The char recession measurements were made at all the calorimeter and shear stress gauge locations that were instrumented on the calibration plate. Since some of the calorimeter and shear stress gauges were close to each other, the shear stress and total heating rate values were inferred based on proximity. The total char recession at each of these sensor locations due to HGF testing was divided by the total test duration to estimate the recession rates. Figure 26 shows a linear trend in char recession rate with increasing total heat flux. There was data scatter, but a qualitative linear trend could be assessed from this plot. There appeared to be a heating threshold point of about 4 BFS where the cork char recession rates began to linearly increase with heat rate and below this threshold the recession rate was approximately zero.

Figure 27 shows char recession rate measurements as a function of wall shear stress measurements for 8 charred cork samples. It was seen that the char recession rate vs. shear stress curves had a bimodal distribution where there was one trend for total heating rates greater than 10 BFS and another distribution below 5 BFS. The recession rate for total heating trends above 10 BFS showed an increase in recession rates above a shear stress of 0.4 psf which then approached an asymptote above a shear stress of 1 psf (red curve in Figure 27). This asymptotic behavior was expected since there was only a finite char layer developed during the TVC cork combustion process which was then stripped away by the high shear and heating environments from HGF testing. Based on the limited dataset available, the char recession rate transition or threshold point occurred at a shear stress of 0.4 psf at high heating environments. Low heating environments less than 5 BFS led to a low constant char recession rate over large range in shear stress (blue curve in Figure 27).

It should be noted that the conservative recession rate was calculated by recording the char recession measurements with the addition of the char layer. The char layer and the pyrolytic zonal layer (where easily defined) were measured by X-Ray CT imaging analysis at each calibration sensor location. This thickness was then divided by the total test duration to obtain the conservative recession rate. Conservative recession rate was determined by stripping the TPS sample from the pre-HGF testing thickness down to just the post-HGF testing virgin layer. The modified HGF char recession test results were compared to the heritage HGF results for virgin P50 cork. The conservative recession rate was applied to both sets of data from the virgin cork (heritage source) and cork char (this study) samples. The conservative recession rates for cork char were considerably higher than for virgin cork for total heating rates and wall shear stress greater than 4 BFS and 0.4 psf, respectively. This suggested that the cork char layer was quite friable to flight environments when the threshold was exceeded and would ablate/erode readily. Understanding the structural integrity of the char layer was critical in estimating TPS performance.

Based on the recession/erosion characteristics of the cork char observed from Figures 26 - 27, a hypothesis on the high char erosion/recession rates were postulated using the schematic shown in Figure 28. This schematic shows the interplay of heating, shear and pressure within the TPS material and freestream. As noted in Figure 26, it was seen that the heating rates had a first order impact on char recession. There was a shear stress threshold which led to a shear load which could mechanically erode the char layer as shown in Figure 27. Mechanical erosion of the char layer was clearly observed by the X-Ray CT scans shown in Figure 29 and Appendix A. Heating rates of greater than 10 BFS and above the shear stress threshold led to almost full erosion of the char layer. X-Ray CT at these heating rates, but shear stress on the order of 1 psf resulted in the entire char layer being stripped away with a very small rind of char layer formed (Figure A1). At very low heat rates and high shear stress, the cork char structural integrity was maintained, and minimal erosion was observed from both Figures 26, 27 and 29. The theory is that as the pyrolytic gases were being formed due to external heating and the TPS pore pressure increased relative to its' surface pressure (*dP/dy* increases), this induced a normal force load on the char layer from the bottom of the char. This pressure gradient further increased as the TPS surface pressure decreased as observed during ascent flight. The TPS surface pressure from HGF was on the order of 2.2 psia for the Mach 0.1 test runs and 4.9 psia for the Mach 0.6 to Mach 0.8 test runs based on the calibration plate measurements. This normal force load outward on the char enabled a small shear load to easily liberate and erode the char layer. Without this internal normal force load induced by surface heating, shear loads above a threshold were not able to strip the char layer from the pyrolytic zone. This suggested that both total heating rates, shear stress and the surface pressure were drivers in mechanical shear erosion of the char layer.

Wall shear stress may play an additional role in char formation and recession. Wall shear stress in the HGF may have resulted in removal of hot pyrolytic sublayer gases from the char surface and dilution with a cooler air freestream, decreasing the surface temperature[15]. This did not consider the cork combustion process and assumed cooler gases flowing over the panels which may apply for flight regimes at certain regions in the base during choked flow. More likely, plume recirculation will remove the hot pyrolytic gas from acting like an insulating layer above the TPS and penetrate heat into the virgin cork layer. These processes led to increasing the temperature gradient (*dT/dy*) normal to the char surface which resulted in a sustained convective heat flux to the TPS char layer and an increase in the char formation rates as shown in Figure 30. Char formation rates were estimated by looking at the post-HGF char depth to pre-HGF char depth ratios. Post-HGF char depths were calculated from Equation 12 where the first term was the char depth measured from X-Ray CT from post-HGF testing ($d_{c,\ post\text{-}HGF}$), and the second term was an integration of the char recession rate ($\dot{r}$) over the test duration. The addition of both terms was an estimate of the total char depth observed during HGF testing. Ratios above one showed that there was char formation occurring during HGF testing. Ratios of near zero suggested that limited to no char formation was occurring. Ratios below one also suggested minor char swelling or some data scatter. Above a total heating rate of 10 BFS and a wall shear stress of 1.3 psf, it was observed that the char formation rates increased. This showed that as the shear was mechanically eroding the char layer and removing the sublayer pyrolytic gas, the heat was penetrating the internal TPS pyrolytic zones and virgin cork and developing additional char when the heating threshold was satisfied. This was a positive feedback loop which led to further P50 cork recession.

According to Smith et al., cork char failure density was characterized in development of their cork recession models[14]. The virgin cork density is approximately 32 lb_m/ft^3. The cork char failure density is demonstrated to be 4.75 lb_m/ft^3 through arc-jet testing[14]. According to the X-Ray CT (shown in Figures 25 and 30) for Run 4, the X-Ray intensity map in the char pixels was 1/7 the intensity map of the virgin cork layer. Cork combustion dynamics resulted in relative char density reaching the char failure density. This was a qualitative assessment since reference known char

densities were not obtained prior to this test program. Hence, currently absolute densities cannot be reported. Highly friable cork char receded rapidly due to heat, pressure and shear loads as noted for Runs 1 – 4 and 8.

The alligator surface cork char topology was observed in both the sub-scale post-TVC ground test and the flight-scale Green Run Hot-Fire 2 test (Figure 31)[1]. This demonstrated that sub-scale TPS panel length scales did not induce other flow physics that were not captured in flight. Surface cork char topology at both scales showed large honeycomb cell diameter structure where shear stress loads were minimal. Pre-HGF Run 5 and Green Run Hot-Fire 2 post-test TPS samples both showed this characteristic char topology of a radiant heating dominant exposure with minimal flow shearing. This observation also substantiated the Green Run data-derived shear stress calculations provided in Figure 12. Through high shear stress and heating rates, this substantially reduced the cork char honeycomb cell diameter structure. This cell structure was of uniform diameter throughout the TPS charred panel due to potentially high shear loads. Further efforts need to be conducted as to the reasoning of these observations.

This study provided rationale that the TPS response to Green Run base environments would be substantially different for flight. There was extensive charring, but no char recession observed from Green Run as noted by various post-test measurements. This HGF test series showed that flight shear and normalized heating environments imposed on cork char, derived by the combustion phenomena, led to significant recession when the threshold criteria were satisfied. The Artemis I SLS flight conditions satisfied these defined thresholds during the cork combustion and peak recirculation regimes. However, spacecraft reentry environments and in-space burns could witness wall shear stress and heating rates above the defined threshold points. Such induced environments for spacecraft and landers with a cork ablator should adequately consider TPS response when selecting TPS type and sizing.

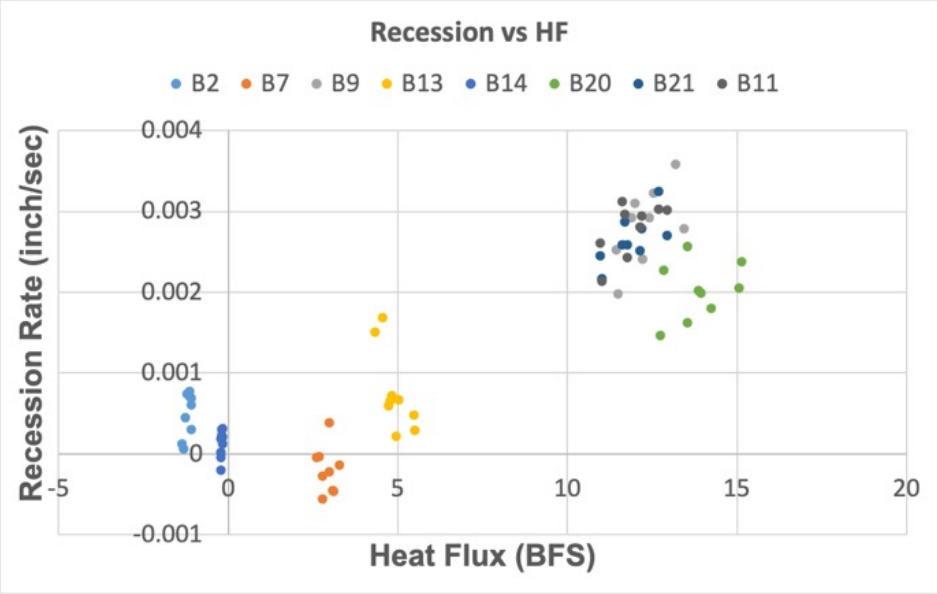

Figure 26. Char recession rate vs. applied heat flux.

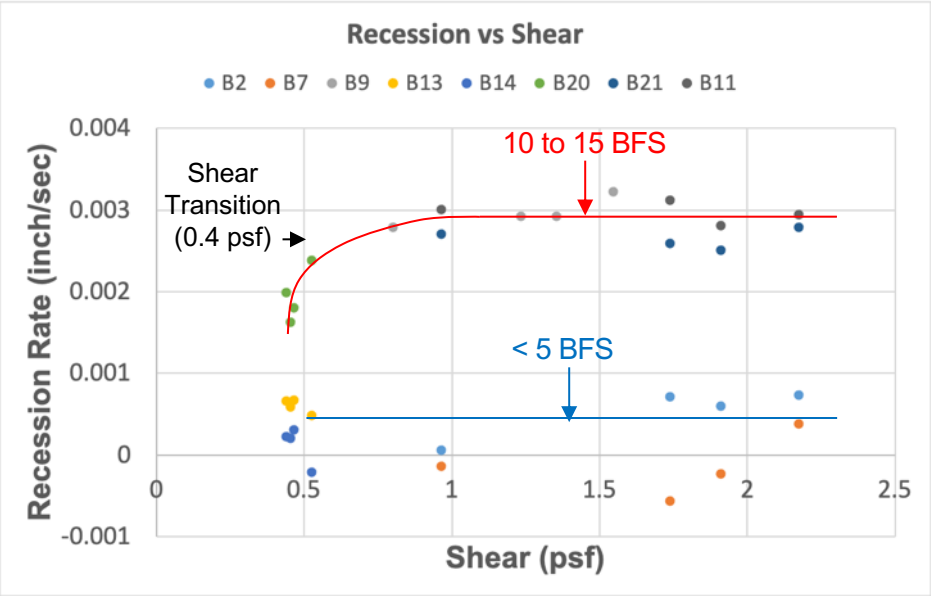

Figure 27. Char recession rate vs. applied wall shear stress.

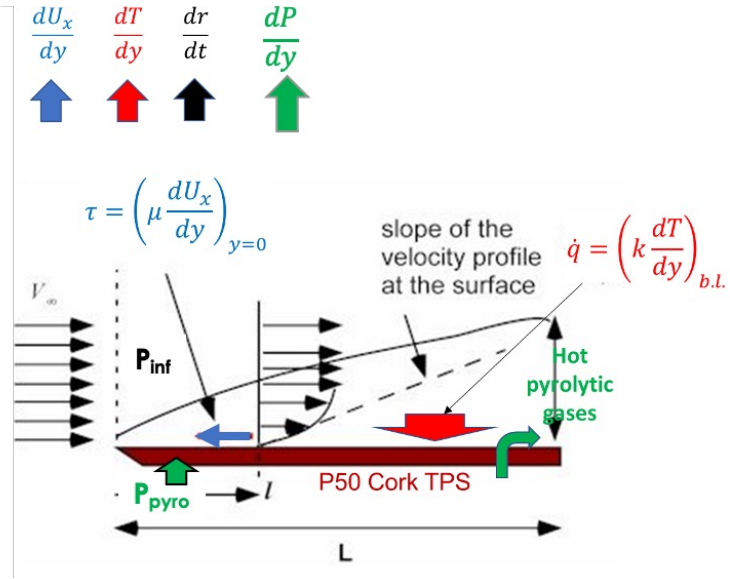

Figure 28. Schematic of the flow physics observed with a TPS ablator.

$$Post\ HGF\ Char = d_{c,post-HGF} + \int_0^{t_f} \dot{r} dt \qquad (12)$$

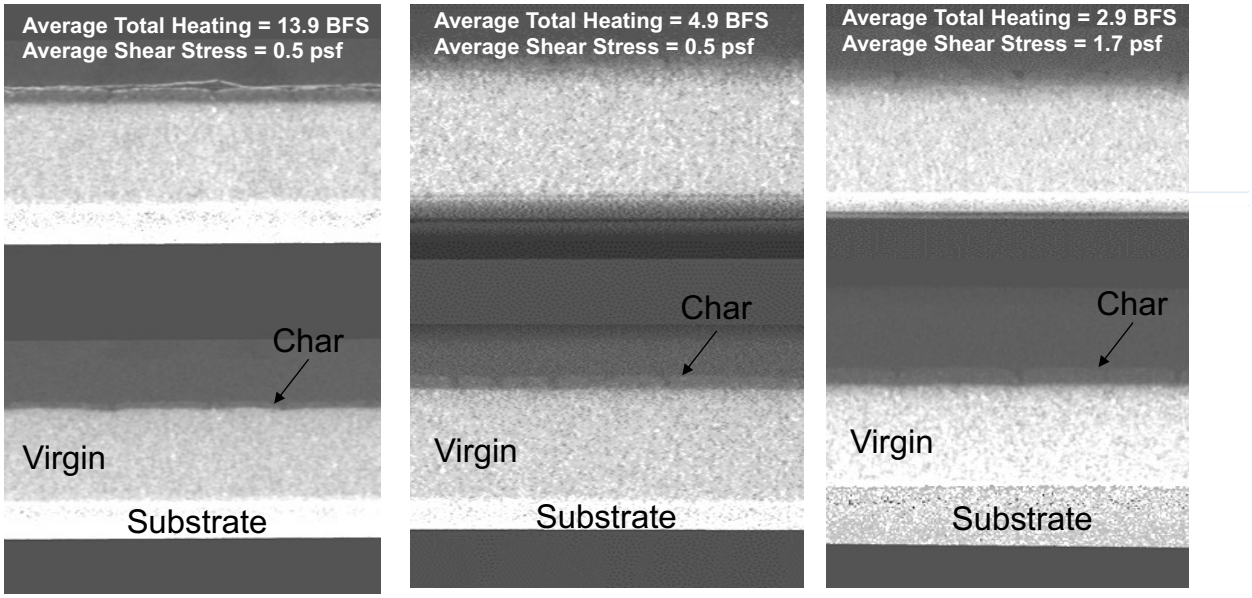

Figure 29. X-Ray CT images of the effects of applied heat flux and shear stress to the P50 cork char and virgin layers. Pre-HGF test scans (top) and post-HGF test scans (bottom).

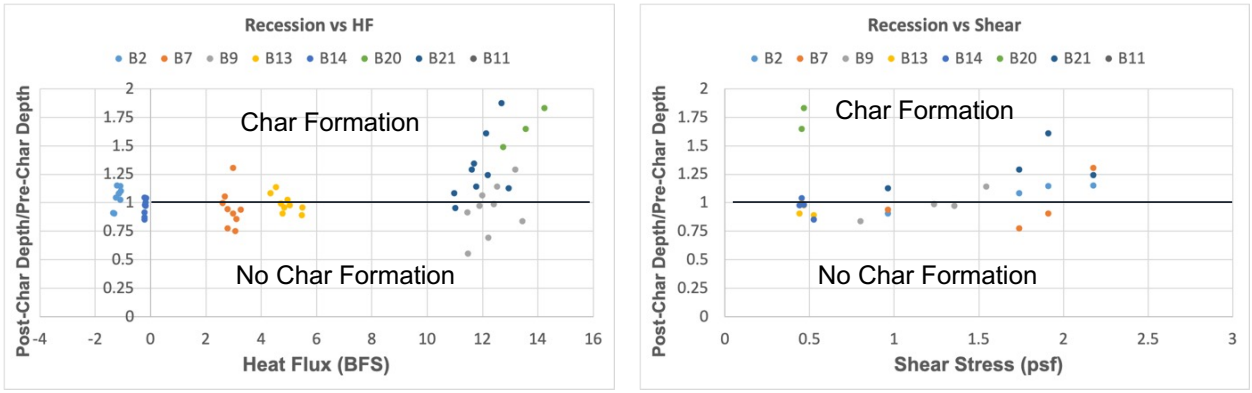

Figure 30. Post-test to pre-test char depth ratio as a function of applied heat flux (left) and wall shear stress (right) conducted at the HGF.

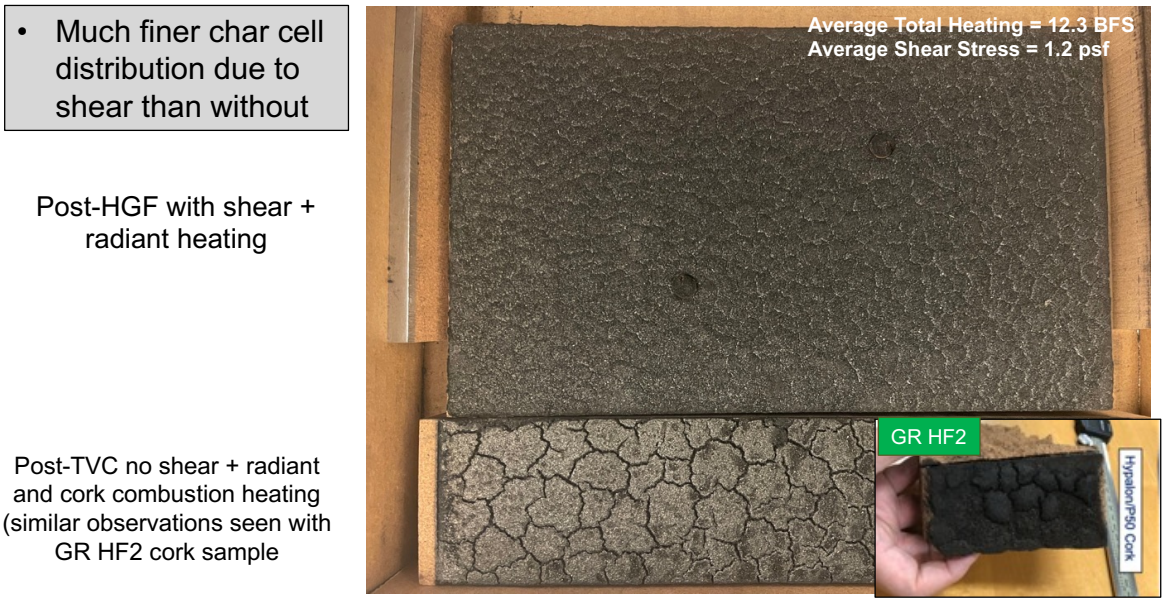

Figure 31. Visible imagery data of post-HGF TPS P50 cork char surface with wall shear stress (top) and without wall shear stress (bottom) including Green Run Hot-Fire 2 P50 cork sample[1].

VI. Conclusions

This investigation tried to uncover the characterization of P50 cork char to ascent flight shear and heating environments due to P50 cork combustion and other base flow regimes. This was to more accurately assess TPS performance for launch vehicles and spacecraft where such an ablator was being used. This investigation first derived flight shear environments from DFI data using isentropic flow theory and the Reynolds-Colburn correlations. Relatively good agreement in wall shear stress is observed between flight data derived methodology and computational simulations for the SLS vehicle. The heritage HGF operation led to significantly higher wall shear stress than flight and as a result a modified operation of the HGF was developed which matched the flight shear and normalized heat transfer parameter environments.

This second component of this investigation was for the test data to define the total heating and shear stress thresholds where cork char was readily liberated. This also enabled the X-Ray CT scans to determine the effects of the flight environments on the char layer and pyrolytic zone topology and to more accurately estimate char recession and char depth. This test data developed a theory on the sources for cork char recession and formation rates. There was a historical approach in estimating the cork recession by assuming that the entire char and pyrolytic zonal layers were ablated in determining TPS sizing. This general approach was conservative in sizing TPS, but this test data suggested that these estimations were valid for the cork ablator and this historical approach did not lead to excessive conservatism in TPS design. Based on this test data, a more accurate assessment of TPS recession on the Core Stage base heat shield and solid rocket booster could be estimated going forward. The main conclusion derived was that when the heating and shear stress thresholds were exceeded, this led to significant erosion of the cork char layer. Cork char was friable and did not maintain its structural integrity when heated through the cork combustion process and potentially other heating mechanisms. Hence, the importance of understanding the cork combustion dynamics for SLS flight which increases TPS convective heating and char depth during ascent. Reentry spacecraft, landers and other upper-stage vehicles where the cork ablator is being used should consider such observations in predicting TPS performance.

Additional work can be done to characterize SLS base wall shear stress comparisons between high-fidelity large-eddy simulation (LES) CFD calculations and flight-data derived results. Additional test points at a shear stress between 0.5 psf and 0.1 psf to further characterize the shear stress threshold and heating rates between 5 BFS and 10 BFS. True shear stress threshold point may not accurately be defined in this test, and it would be ideal to confirm recession rates at lower shear stress values.

Appendix A: Additional X-Ray CT and Visual Imagery Data Sets

Figure A1 shows the X-Ray CT scan of one of the highest applied heating rates and shear stress on the TPS sample. This led to the uniform mechanical erosion of the entire char layer, leaving a cork char rind of minute thickness on the surface. Figures A2 and A3 show visible imagery datasets of the side and top-down views of the pre-HGF and post-HGF test TPS panels for Runs 1 – 3, 5 – 6 and 8.

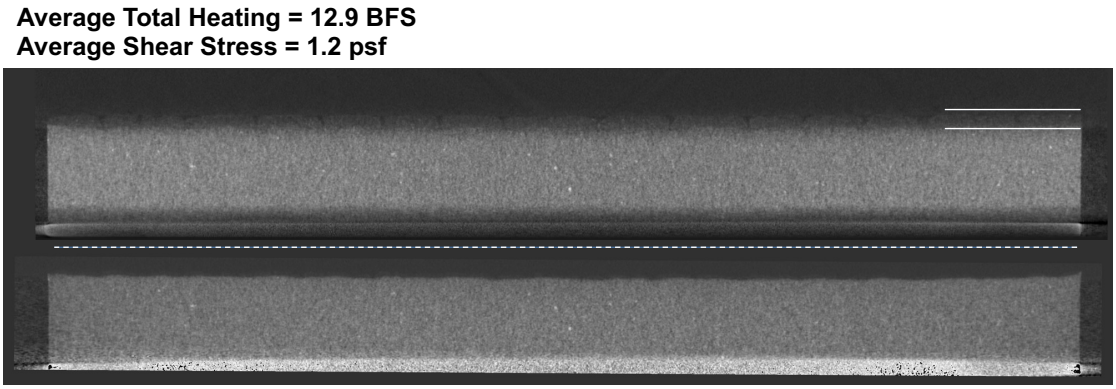

Figure A1. HGF Run 8: Pre-HGF test TPS sample side view X-Ray CT image (top); two white solid lines show char depth from P50 cork combustion process within the TVC (top) and post-HGF test TPS sample X-Ray CT image (bottom); dashed white line shows the initial top-surface of the pre-HGF test TPS (bottom).

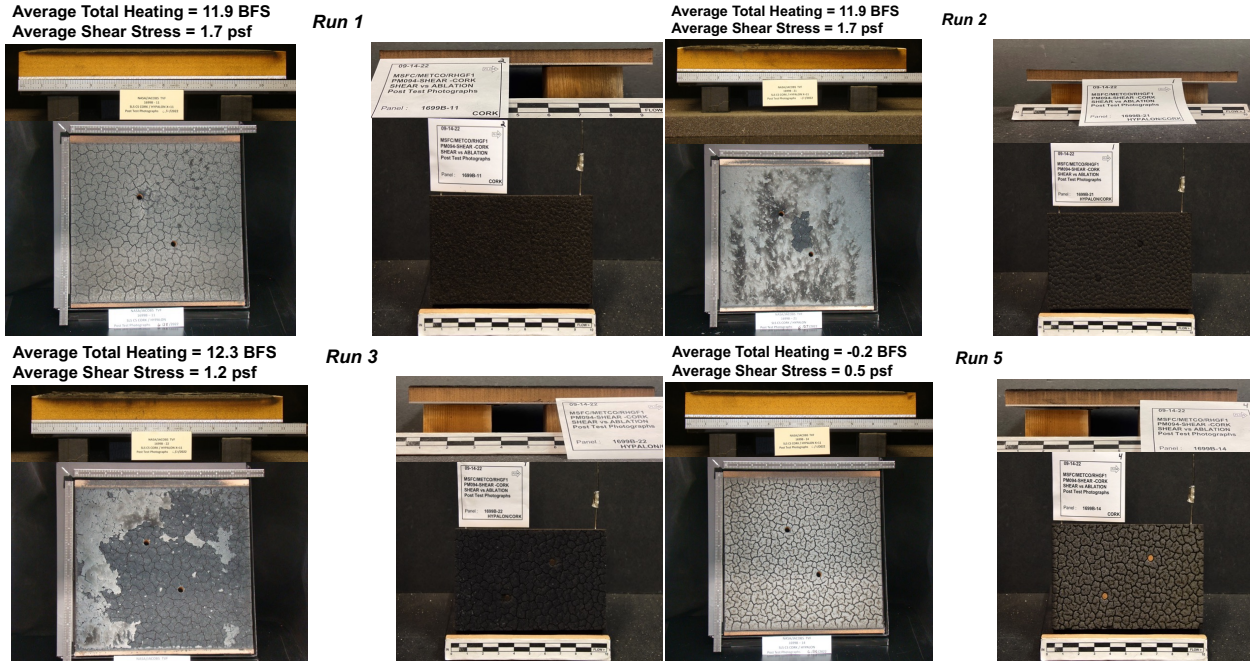

Figure A2. HGF Runs 1-3 and 5: Pre-HGF test TPS sample top-down and side images (left) and post-HGF test TPS sample images.

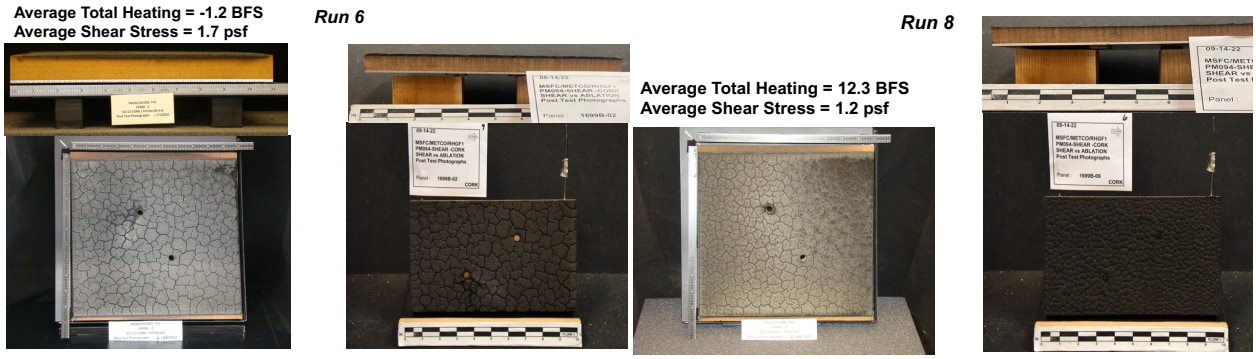

Figure A3. HGF Runs 6 and 8: Pre-HGF test TPS sample top-down and side images (left) and post-HGF test TPS sample images.

Acknowledgements

Thanks to the efforts of the technical staff within the NASA Marshall Space Flight Center's Aerosciences Branch such as Dr. Chris Morris, Dr. Francisco Canabal, Liz Suttles and Brandon Mobley for data review and flow physics insight and the Propulsion Test Branch for access to the Hot Gas Facility, testing, data collection and handling of the TPS specimens. Contributions from the Damage Tolerance Branch in access to their facilities and X-Ray systems have been extremely beneficial in evaluating the TPS response and characterization. Valuable guidance and assistance from Darrell Davis of the MSFC Thermal Analysis and Control Branch was also provided. This testing was supported by Michael Alldredge and Eric Vanderslice of the SLS Stages Office and Janet Sisk of the Structural Design and Analysis Division within the MSFC Spacecraft and Vehicle Systems Department.

References

[1]Mehta, M., C.I. Morris, B.L. Mobley and T.L Prickett., "Space Launch System Core Stage Green Run Base Heating: Anomaly, Mitigation and Flight Redesign," *AIAA SCITECH 2023 Forum*, American Institute of Aeronautics and Astronautics, 2023. https://doi.org/10.2514/6.2023-0644

[2]Mehta, M., B.L. Mobley and S.D. Smith., "Space Launch System Base Aerothermodynamics Post-Flight Reconstruction for Artemis I," *AIAA SCITECH 2024 Forum*, American Institute of Aeronautics and Astronautics, 2024. https://doi.org/10.2514/6.2024-0256

[3]Mehta, M. and T.B. Steva, "Space Launch System Base Aerodynamics Post-Flight Reconstruction for Artemis I," *AIAA SCITECH 2024 Forum*, American Institute of Aeronautics and Astronautics, 2024. https://doi.org/10.2514/6.2024-0257

[4]Morris, C.I. (2015), "Space Launch System Ascent Aerothermal Environments Methodology", *53rd AIAA Aerospace Sciences Meeting, AIAA SciTech*, (AIAA 2015-0561), Kissimmee, FL. https://doi.org/10.2514/6.2015-0561

[5]Scott, C.F. and J.A. Inman, "SCIFLI Airborne Observation of the Hayabusa2 Sample Return Capsule Re-Entry", *AIAA AVIATION 2022 Forum,* American Institute of Aeronautics and Astronautics, 2022, https://doi.org/10.2514/6.2022-3798

[6]Mehta, M., Dufrene, A. T., Seaford, M., and Knox, K., "Space Launch System Base Heating Test: Environments and Base Flow Physics," *54th AIAA Aerospace Sciences Meeting*, American Institute of Aeronautics and Astronautics. https://doi.org/10.2514/6.2016-0547

[7]MEDTHERM Corporation, "64-Series Heat Flux Transducers and Infrared Radiometers for the Direct Measurement of Heat Transfer Rates", Bulletin 118, MEDTHERM Co, Huntsville, AL, 2002.

[8]Shrestha, P., Hill, J., Simmons, D., and Meritt, R.J.., "Comparison between computational and experimental wall-shear stress and pressure measurements in a supersonic wind tunnel", 2022 *AIAA Aviation Forum*, American Institute of Aeronautics and Astronautics, 2022. https://doi.org/10.2514/6.2022-3677

[9]Mehta, M., D.A. Brewer, R.D. Beshears, G.C. McDougal and E.S. Schofield, "Thermal protection system P50 cork environments and response due to radiative heating," *AIAA SCITECH 2025 Forum*, American Institute of Aeronautics and Astronautics, 2025. https://doi.org/10.2514/6.2024-0256

[10]Mullen, C.R., et al. 1972. *Saturn Base Heating Handbook*. Final Report, NASA CR-61390. Washington DC: National Aeronautics and Space Administration.

[11]Goethert, B.H., 1960. Base Flow Characteristics of Missiles with Cluster-Rocket Exhausts. Institute of Aeronautical Sciences Paper No. 60-89

[12]Chemical Propulsion Information Agency (CPIA). 1981. *JANNAF Handbook, 1981, Rocket Exhaust Plume Technology*. Publication 263. Chemical Propulsion Information Agency (CPIA).

[13]Neumann, R.D. and J.R. Hayes. 1986. Introduction to Aerodynamic Heating of Supersonic Missiles, Tactical Missile Aerodynamics. *Progress in Astronautics and Aeronautics.* 104:421–481.

[14]Smith, E., B. Lamb, R. Beck and E. Fretter (1992), "Thermal/Ablation Model of Low-Density Cork Phenolic for the Titan IV Stage I Engine Thermal Protection System", AIAA 92-2905, Nashville, TN

[15]Lienhard, J.H. and J.H. Lienhard (2020). A Heat Transfer Textbook, Phlogiston Press, Cambridge, MA.

[16]McBride, B.J. and S. Gordon (1996), Computer Program for Calculation of Complex Chemical Equilibrium Compositions and Applications, NASA-RP-131, NASA Glenn Research Center, Cleveland, OH.